Metabolome segregation of four strains of *Saccharomyces cerevisiae*, *S. uvarum* and *S. kudriavzevii* conducted under low temperature oenological conditions.

Romain Minebois[a], Roberto Pérez-Torrado[a] and Amparo Querol[a]*

[a]Instituto de Agroquímica y Tecnología de los Alimentos, IATA-CSIC. E-46980 Paterna, Spain.

Summary

The monitoring of fermentation at low temperatures (12-15ºC) is a current practice in the winery for retention and enhancement of the flavour volatile content of wines. Among *Saccharomyces* species, *S. uvarum* and *S. kudriavzevii* have revealed interesting industrial properties, including better adaptation at low temperatures. To gather deeper knowledge of the fermentative metabolism at a low temperature of these species together with *S. cerevisiae*, we performed a comparative metabolomic analysis using four representative strains. We used batch cultures to obtain an exhaustive and dynamic image of the metabolome of strains passing through the sequential stresses related to the winemaking environment. A great variety of intra- and extracellular metabolites (>500 compounds) were quantified across fermentation using distinct chromatographic methods. Besides a global decrease in the lipid composition of the four strains when they entered into the stationary phase, we reported some strain-specific high magnitude changes. Examples of these differences included divergent patterns of

This article has been accepted for publication and undergone full peer review but has not been through the copyediting, typesetting, pagination and proofreading process which may lead to differences between this version and the Version of Record. Please cite this article as doi: 10.1111/1462-2920.15135

production of short-chain fatty acids and erythritol in the *S. uvarum* strain. Strains also differed in expression for aromatic amino acid biosynthesis and sulphur metabolism, including the glutathione pathway. These data will allow us to refine and obtain the most value of fermentations with this alternative *Saccharomyces* species.

Introduction

In winemaking, fermentation temperature and yeast strains are two critical parameters that govern the final organoleptic qualities of wine. The use of low temperatures (12-15ºC) during fermentation is a current practice in the winery. It enables not only retention but also enhancement of the flavour volatile content of wines (Molina *et al.*, 2007). Nowadays *S. cerevisiae* is the most important yeast involved in wine fermentation. However, *S. cerevisiae* has an optimal growth temperature around 32ºC, which supposes some disadvantages for the winemakers when fermenting at low temperatures (12-15ºC). For instance, the lag phase of *S. cerevisiae* increases, and its growth rate decreases, which can lead to prolong the duration of the process with a greater risk of halted or sluggish fermentation (Blateyron and Sablayrolles, 2001).

Consequently, the finding of new *Saccharomyces* and non-*Saccharomyces* yeasts able to correctly ferment in low temperature environments has been in the spotlight of worldwide wine yeast research over the past few years (Pérez-Torrado *et al.*, 2018). Within the *Saccharomyces* genus, this is the case of the cryotolerant yeasts *S. uvarum* and *S. kudriavzevii*. *S. kudriavzevii* has been isolated only from natural environments (Sampaio and Gonçalves, 2008; Lopes *et al.*, 2010), most likely because of its poor ethanol resistance (Belloch *et al.*, 2008). On the contrary, *S. uvarum* has been

mainly isolated from fermentation at cold temperatures (Naumov *et al.*, 2000; Demuyter *et al.*, 2004; Tosi *et al.*, 2009; Masneuf-Pomarède *et al.*, 2010). Previous physiological and oenological characterisations of *S. uvarum* and *S. kudriavzevii* strains have demonstrated their potential for fermenting wine musts at low temperatures. For instance, Masneuf-Pomarède *et al.* (2010) demonstrated that several strains of *S. uvarum* were able to complete alcoholic fermentation at 13ºC faster than commercial *S. cerevisiae* strains. Regarding *S. kudriavzevii*, because even at low temperature, *S. cerevisiae* is the most fermentative competitive species, overall hybrids *S. cerevisiae x S. kudriavzevii* have revealed interesting technological applications (Peris *et al.*, 2016, 2018). Likewise, both *S. uvarum* and *S. kudriavzevii* species have additional advantages as compared to *S. cerevisiae* in terms of organoleptic properties, such as greater glycerol production, and lower ethanol synthesis (Arroyo-López *et al.*, 2010; Varela *et al.*, 2016). However, up-to day there are still very few studies that aimed to deeper understand the metabolism of *S. uvarum* and *S. kudriavzevii*, and particularly at low fermentation temperatures. From an industrial outlook, such knowledge is necessary to develop better hybridization and metabolic engineering strategies that look at the role of genes and pathways on cold adaptation.

High-throughput experimental techniques, also called omics techniques, represent valuable tools to investigate in-depth how an environmental parameter, like temperature, can impact the variety of cellular processes and the phenotype characteristics in *Saccharomyces* species. Comparative transcriptomic studies at high (25-28ºC) and low temperatures (12-15ºC) have shown that the enhanced production of

fermentative aromas in *S. cerevisiae*, *S. uvarum* and *S. kudriavzevii* at low temperatures may be due in part to differential expression of genes implicated in their synthesis, e.g., genes involved in the catabolism of amino acids by the Ehrlich pathway and in the degradation of branched chain amino acids (Beltran *et al.*, 2006; Gamero *et al.*, 2014). Another transcriptomic work also suggested that *S. kudriavzevii* strains had enhanced their translation efficiency as an adaptive mechanism to better grow at low temperatures (Tronchoni *et al*., 2014). Moreover, a recent proteomic study has shown that genes and proteins involved in lipid metabolism belong to one of the metabolic groups most affected by low temperatures in *S. cerevisiae*, *S. uvarum*, and *S. kudriavzevii* (García-Ríos *et al.*, 2016). Regarding metabolomics studies, López-Malo *et al.* (2013) offered a first detailed metabolic comparison between *S. cerevisiae*, *S. uvarum*, and *S. kudriavzevii* performed in chemostat culture at 12ºC. In the latter study, strains were grown at a dilution rate fitting the initial exponential phase of wine fermentation, and the authors found that the main differences among the four species were in carbohydrate metabolism, especially fructose metabolism. Likewise, they found that *S. uvarum* presented elevated shikimate pathway flux, while *S. kudriavzevii* displayed increased NAD+ synthesis at 12ºC.

In most of the aforementioned studies, experiments were conducted in chemostat cultures. Chemostat cultures enable precise control of specific growth rate and, at steady-state, the concentrations of all metabolites, substrates, and culture variables (pH, temperature, and oxygen availability) are constant in time. Thus, chemostat steady-states cultures are convenient for the study of prolonged exposure to low temperature

and the identification of gene expression, proteome profiles, or specific pathway activity. However, wine fermentations are traditionally conducted in batch mode, which can be regarded as unfavourable conditions for yeast growth since yeast cells are subjected to various and sequential stresses (Matallana and Aranda, 2017). During alcoholic fermentation, yeasts go through a lag phase, a growth phase, and a stationary phase during which more than half of the sugar is fermented. A complete study of yeast physiology under winemaking conditions must, therefore, include yeasts in a non-growing phase. This condition is impossible to achieve within a chemostat (Clement *et al.*, 2011). Besides, in batch fermentations, culture variables, extra- and intracellular metabolites and biomass evolve over time. This makes batch cultures more suitable to study the dynamics of adaptation to low temperature and the identification of changes in metabolic pathways across time. Accordingly, in an attempt to identify inter-specific metabolic differences between *S. cerevisiae*, *S. uvarum,* and *S. kudriavzevii* at high fermentation temperature, we recently performed a metabolomic comparison using batch fermentations at 25ºC (Minebois *et al.*, 2020). We observed interesting variations among four strains of *S. cerevisiae*, *S. uvarum,* and *S. kudriavzevii* for the consumption of some nitrogenous compounds and in the levels of some metabolites involved in redox homeostasis such as succinate, glycerol, and 2,3 butanediol. The most important differences were found in *S. uvarum* strains. For instance, the two *S. uvarum* strains used were characterized by a “production-consumption” profile of extracellular acetate that we hypothetically associated with lipids synthesis and membrane remodelling. Also, we found some evidence that *S. uvarum* strains were metabolically more active

than *S. cerevisiae* strains through the pentose phosphate pathway when entering into the stationary phase as demonstrated by a higher erythritol synthesis, a downstream metabolite of this pathway. On the contrary, because the *S. kudriavzevii* strain had a very important shortcoming in growth at 25ºC, the identification of clear metabolic strategies was limited.

On the first hand, the present work aimed to encounter inter-specific metabolic differences between *S. cerevisiae*, *S. uvarum*, and *S. kudriavzevii* at low fermentation temperature (12ºC). We selected four yeast strains, including one winemaking strain of *S. cerevisiae* (T73), one natural-isolate of *S. cerevisiae* (YPS128), one winemaking strain of *S. uvarum* (BMV58), and one natural-isolate of *S. kudriavzevii* (CR85). On the other hand, because strains T73, BMV58, and CR85 were previously characterized at 25ºC using a similar methodology (Minebois *et al.*, 2020), we also tried to discern intra-specific metabolomic strategies between low (12ºC) and high temperature (25ºC). From the large intra- and extracellular metabolites data set we obtained (>500 compounds), we proceeded to a thorough inspection of the general pathways and time trends that could differentiate the strains. We looked for performance differences between the strains based on their utilization or production of various compounds over time, in the context of their biochemical pathway associations and the evolution of the environmental parameters.

Results

In this work, we performed an in-depth study of the metabolic behaviour of four yeast strains at 12ºC under winemaking conditions. The wine strain T73 and the wild strain YPS128 belong to *S. cerevisiae* species, while strain BMV58 and strain CR858 belong to *S. uvarum* and *S. kudriavzevii* species respectively. An overview of the fermentation course with the kinetics of the main fermentative parameters (OD_{600}, dissolved oxygen, YAN, carbon dioxide release, sugar consumption, and ethanol production) is presented in **Figure 1A** for each strain. Also, the extracellular concentration of the principal compounds accounting for YAN, namely ammonia, arginine, and glutamine, as well as the extracellular proline content are presented below in **Figure 1B**. We compared the growth capacity and the kinetics of the main fermentative by-products (ethanol, glycerol, succinate, 2,3 butanediol, acetate, and erythritol) generated through the central carbon metabolism (CCM) of yeasts at 12ºC. To do so, the experimental data of OD_{600}, biomass, YAN, and the by-products cited above were fitted to distinct mathematical equations as described in the material and methods section. The fermentative parameters calculated from models are listed in **Table 1**.

General fermentation performances

As shown in **Figure 1A**, fermentations were completed between 430 and 550 hours, being T73 and BMV58 the first strains in this order to reach a dry white wine composition (<4g/l of residual sugars). Even if the *S. cerevisiae* strain YPS128 was the quickest in initiating alcoholic fermentation as shown by its shorter lag phase (**Table 1**), it did not consume the totality of sugars (**Figure 1A**). Regarding biomass production,

BMV58 and YPS128 strains had the highest dry weight biomass values followed by T73 and CR85 strains (**Table 1**). Intriguingly, CR85 did not consume the totality of ammonium and arginine (**Figure 1B**), which could partially explain its lower biomass production. This inability of strain CR85 to totally consume arginine was also observed at 25ºC (Minebois *et al.*, 2020), which suggests that temperature is not the main parameter that influences arginine catabolism in CR85.

The average diameter of cells (ACD) throughout the fermentation was determined and is presented in **Figure 2** . Cells of strain CR85 were overall as bigger as cells of strains T73 and YPS128. On the contrary, BMV58 cells were mostly smaller than the cells of the rest of the strains. Moreover, the comparison of the timing of lag phase, dissolved oxygen depletion, and nitrogen starvation with ACD trends (**Figure 2**) suggested that ACD could be used as another indicator of the fermentation stage, as we previously observed (Minebois *et al.*, 2020).

Finally, a principal component analysis (**Figure 3**) was used to provide a general overview of the data set from **Table 1** which included the 6 growth and the 12 by-products variables. The four yeasts were mostly separated through the first axis which accounted for 36.73% of the total variation and was mainly defined by the correlated variables T_{50}YAN, Eth_{max} and $But_{max,}$ and the negatively correlated variable r_{Ery}. On the other hand, the final content of acetate and succinate, Ac_{max} and $Succ_{max}$, the maximum rate of butanediol, r_{But}, and the majority of the growth parameters (g_{DW}/g_{YAN}, DW_{max} and μ_{max}) were the variables that most contributed to the second principal component explaining 30.96% of the variance. In this defined space, strain T73 was separated from

other strains, mainly because of its high acetate production and also due to its low biomass yield at 12ºC. Interestingly, the cryotolerant strains CR85 and BMV58 did not exactly cluster together, which was explained by differences in their by-products and biomass yields. The *S. kudriavzevii* strain was mainly associated with high butanediol and ethanol content (But_{max} and Eth_{max}), slow nitrogen consumption ($T_{50}YAN$), and low biomass production (DW_{max}). On the contrary BMV58 strain segregated to the negative part of the y-axis by its high biomass yield, high succinate, and low acetate production. However, both CR85 and BMV58 strains clustered in the bottom right-hand corner respectively, which included the variables associated with low temperature and osmotic regulation strategies, for instance, high glycerol and high erythritol production (Gly_{max} and Ery_{max}). Finally, the natural isolate of *S. cerevisiae* had an intermediate position between T73 and BMV58 strains on this PCA projection. Indeed, YPS128 strain had a good biomass yield at 12ºC as well as lower acetate content in comparison to the *S. cerevisiae* wine strain.

Extracellular and intracellular metabolomes comparison

The intra- and extracellular metabolomes were quantified along the fermentation process. Four sampling points which corresponded to growth phase (GP), end of growth phase (EGP), early stationary phase (ESP) and mid-stationary phase (MSP) were used to determine the intracellular metabolomes of each strain, while extracellular metabolomes were determined from tens points distributed from the beginning to the end of the fermentation (**Figure 1A**). Because the strains were grown under different time regimes it was not possible to compare them in a direct statistical manner.

However, for both intra- and extracellular metabolomes, we attempted to discern the general pathways and time trends that differentiated the four strains. When possible, intra- and extracellular data were combined to detail specific pathway observations among the four strains.

Strain-specific intracellular metabolomes observations

The principal component analysis presented in **Figure 4A** was obtained from intracellular triplicates samples. As shown in **Figure 4A**, the triplicates tended to cluster closely and all samples segregated strongly by both strains (**Figure 4A left graph**) and time (**Figure 4A right graph**). Separation by time accounted for the first component variance, while separation by strains was apparent in both the second and third components. Regarding the segregation by strains, only the earliest time points for BMV58 and YPS128 showed any overlap. Considering time segregation, we saw that the widest separation was between GP and EGP time points. For instance, we noticed a strong decrease in many lipids after the first time point in each strain (**Figure S1**). The third (ESP) and fourth (MSP) time points were more closely associated, although fully separated except for one sample in the BMV58 group. Another way to judge the magnitude of metabolic effects caused by specific variables was to summarize the number of compounds significantly changed ($p \leq 0.05$) in each pair-wise comparison of intracellular sampling points, and the direction of those changes (**Figure 4B**). Consistent with the PCA analysis above, the vast majority of changes were already apparent at the second time point of intracellular samples (relative to the first time point). Relatively few compounds, in terms of gross numbers, were added in the later

samplings. Also, comparisons of the third and fourth sample times to each other yielded the smallest number of statistically significant differences in most cases.

As stated above, it was not feasible to compare data from the various strains directly. Consequently, we looked for ways to discern differences between the performance of the strains based on their utilization or production of various compounds over time, in the context of their biochemical pathway associations. Due to the very large number of intracellular compounds quantified (>500 compounds), several approaches were attempted as presence vs. absence of a particular compound. As presented in **Figure 5A**, UDP-galactose was not detected in either of the *S. cerevisiae* strains but was present in all the samples of BMV58 and CR85, suggesting *S. uvarum* and *S. kudriavzevii* strains may have different cell wall sugar profiles. On the other hand, N-acetyltryptophan was only present in the *S. cerevisiae* strains. Octanoylcarnitine was found only in BMV58, while eicosanoylsphingosine was absent only in this strain, and ethanolamine was not detected in the *S. kudriavzevii* strain (**Figure 5A**).

Another approach was to evaluate the magnitude of large changes observed during the fermentation and to determine if the strains differed significantly (**Figure 5B**). For instance, one compound with large accumulation was acetylcholine, which reached a 140-fold increase in *S. uvarum*, but was about two orders of magnitude lower than the other strains (**Figure 5B**). Also, we noted that the storage fructan oligosaccharide 1-kestose was apparently differentially utilized by the strains (**Figure 5B**). The compound was found at very similar levels in all strains at the first time point,

but while *S. cerevisiae* T73 and *S. kudriavzevii* CR85 fully depleted this compound, *S. uvarum* BMV58 and *S. cerevisiae* YPS128 did not affect its levels significantly over time, suggesting that these two strains could not utilize this pool of carbon source for fermentation. Moreover, we observed differences in the intracellular level of some short and medium chain fatty acids (from C6 to C14) which might be relevant to wine production. Butanoate (C4) and 3-methyl-butanoate (C5) are considered odorants or flavour compounds in various foods, including wine. Both compounds declined in the *S. cerevisiae* T73 strain over time, but increase slightly in YPS128, and both were highest in the *S. uvarum* strain, increasing over the fermentation time. *S. kudriavzevii* CR85 had low levels that did not change significantly (**Figure 5B**). Also, BMV58 was the only strain that accumulated (almost 4 fold) the medium chain fatty acid myristate (C14). Regarding compounds that showed the greatest accumulation over these fermentations, we found trehalose, followed closely by its immediate precursor trehalose-6-phosphate (T6P), as shown in **Figure 5C**. It accumulated to similarly high levels in all the strains, representing an increase of >260-fold in BMV58 strain. Finally, the tryptophan precursor anthranilate which increased >150-fold in *S. kudriavzevii* was one of the important differences observed among the four strains in the aromatic amino acid pathways (see below).

Differences in succinate and glycerol production pathways

The depletion of dissolved oxygen initially contained in the white must was completed between 30 and 80 hours of fermentation, strain YPS128 being the quickest in consuming oxygen (**Figure 1A**). During this period of time, a decrease in the

extracellular amount of succinate was observed in the four fermentations (**Figure 6**). After oxygen depletion, the extracellular level of succinate remained constant during few hours (T73, BMV58, and CR85 strains) and newly started to increase when yeast cells entered into the stationary phase (**Figure 6**). This extracellular succinate uptake notably coincided with a proline uptake (**Figure 1B**). Besides, extracellular levels of succinate at the end of the fermentation were proportional to the intracellular amounts of each strain. For instance, the highest intracellular accumulation of succinate between the first and the fourth intracellular sampling point was observed in BMV58 strain (>4 fold) and also produced the largest amount of succinate (5.63 $g \cdot l^{-1}$) (**Table 1**, **Figure 6**). In BMV58, the higher succinate synthesis might have contributed to acidification and to decrease the pH level of the final wine (**Figure S2**). In yeasts and in anaerobic conditions, succinate can be generated by the reductive or the oxidative pathway of the tricarboxylic acid cycle (TCA) (**Figure 6**). In accordance with this, the intracellular level of aspartate, a precursor of oxaloacetate, largely decreased between the mid-exponential phase and the advanced stage of the stationary phase in BMV58 (>5.8 fold). Moreover, except in CR85 fermentation, we observed an increase in the intracellular content of the two intermediates of the reductive branch of TCA, malate, and fumarate, between the first and fourth intracellular sampling point in T73, BMV58 and YPS218 strains (**Figure 6**). Regarding the oxidative branch of TCA, the intracellular levels of citrate and isocitrate, both precursors of alpha-ketoglutarate, increased largely during the fermentation in the four strains. Nevertheless, the intracellular amount of alpha-ketoglutarate, which is an important node between CCM and nitrogen metabolism,

behaved very differently among the four strains (**Figure 6**). In CR85 and YPS128 fermentations, the content of this keto-acid showed a small but significant increase, while in T73 fermentation it decreased along the whole fermentation. On the contrary, in BMV58 alpha-ketoglutarate content decreased between GP and EGP and increased between ESP and MSP. Moreover, BMV58 strains had the lowest intracellular glutamate level when entered into the early stationary phase (**Figure 6**). These results suggest that a higher amount of the alpha-ketoglutarate generated through the reductive branch of the TCA could contribute to the succinate production in BMV58 strain, notably during the early stationary phase.

The strains of the cryotolerant species *S. uvarum* and *S. kudriavzevii* produced the largest amount of glycerol (8.22 $g \cdot l^{-1}$ and 7.79 $g \cdot l^{-1}$ respectively) at the end of the fermentation (**Figure 6, Table 1**). On the other hand, T73 and YPS128 *S. cerevisiae* strains produced very similar quantities of glycerol (**Table 1**). Interestingly, if we compare the extracellular amount of glycerol at the time of each intracellular sampling point between the four strains, we can see that it was always equal or higher in BMV58 and CR85 fermentations than in both *S. cerevisiae* strains. In contrast, intracellular levels of glycerol as well as the pathway intermediates, namely DHAP and glycerol-3-phosphate, were higher only in the fourth time point in BMV58 (**Figure 6**). Besides, in strain CR85 the intracellular levels of glycerol-3-phosphate and DHAP were lower than the other strains which produced less glycerol. These observations suggest higher activity as well as increased catalytic properties of the CR85 enzymes involved in the

glycerol pathway, notably the activities involved in DHAP and Glycerol-3-phosphate catabolism as was previously suggested elsewhere (Oliveira et al., 2014).

Differences in acetate metabolism

In our winemaking simulations at 12ºC, the *S. cerevisiae* wine strain T73 produced the largest amount of extracellular acetate (0.43 $g \cdot l^{-1}$) (**Table 1**). On the contrary the natural isolate of *S. cerevisiae*, YPS128 strain produced 2 fold less acetate (0.21 $g \cdot l^{-1}$) than T73, and also less acetate than CR85 strain (0.34 $g \cdot l^{-1}$). Regarding the concentration of acetate in the *S. uvarum* fermentation, we observed a very similar pattern to the one obtained at 25ºC in previous work (Minebois *et al.*, 2020) with BMV58 and another *S. uvarum* strain (CECT12600). BMV58 strain released acetate until the entry into the stationary phase, after which the extracellular amount of acetate started to decrease to reach the lowest value of 0.03 $g \cdot l^{-1}$ (**Figure 6**; **Table 1**).

Acetate is a precursor for the synthesis of acetyl-CoA (**Figure 6**). Here we observed that the intracellular contents of acetyl-CoA in BMV58 and CR85 strains were greater than both *S. cerevisiae* strains (**Figure 6**). In agreement with the latter result, a higher increase in the synthesis of the precursors of acetyl-CoA, pantothenate and CoA compounds, occurred when we compare GP and EGP intracellular sampling points in BMV58 and CR85 strains. Also, we observed that intracellular levels of CoA (BMV58 strain only) and pantothenate (BMV58 and CR85 strains) were higher from the second intracellular sampling point when compared to *S. cerevisiae* strains (**Figure 6**).

Higher activity of pentose phosphate and chorismate pathways in the S. uvarum strain

A clear difference between strains was found for the synthesis of the aromatic amino acids, accomplished through the pentose phosphate and shikimate pathways (**Figure 7**). Bar plots for the various aromatic precursors, including 3-dehydroquinate (>32 fold increase), 3-dehydro-shikimate (>58 fold increase), and shikimate (>3 fold increase), show clearly that the *S. uvarum* strain was much more anabolically active through the shikimate pathway. The proteinogenic aromatic amino acids themselves did not vary among strains (bar plots not shown), but catabolites of phenylalanine such as phenylacetate (>2.9 fold increase) and phenyl lactate (>5 fold increase) appeared to correlate to the precursor levels. Moreover, these results were in accordance with both the timing of production and the higher extracellular levels of phenylpropanoids (2-phenylethanol and 2-phenylethyl acetate) that were quantified in the BMV58 fermentation (see below). Also, as stated above, anthranilate, which is the first committed precursor to the tryptophan pathway, was much higher in *S. kudriavzevii* CR85 (>150 fold), although this did not correlate to tryptophan or its downstream catabolites kynurenine and kynurenate (**Figure 7**).

On the other hand, we previously mentioned that the cryotolerant strains BMV58 and CR85 produced higher levels of erythritol (**Table 1**). Erythritol is an endogenously made compound originated from erythrose-4-phosphate, a pentose phosphate pathway derivative that also serves as a precursor for the shikimate pathway (**Figure 7**). We observed that intracellular levels of erythritol decreased strongly overgrowth for all the strains except for *S. uvarum* strain, where it increased more than two-fold between GP and MSP (**Figure 7**). Moreover, the intracellular levels of

xylulose and ribulose, precursors of xylulose-5-phosphate and ribulose-5-phosphate, were higher in BMV58 (**Figure 7**). The higher intracellular accumulation of erythritol in BMV58 was in agreement with the higher extracellular levels of erythritol found in BMV58. Also, the comparison between the evolution of the intra- and extracellular levels of erythritol in the four strains suggested two different modes of production of this metabolite. T73, YPS128 and CR85 strains accumulated this compound earlier during the fermentation process, probably during the growth phase, and started to release it into the extracellular medium when they entered into the stationary phase. On the contrary, the production of erythritol peaked after entry into the stationary phase in BMV58 (**Figure 1, Figure 7**).

Intracellular metabolism of sulphur

The metabolism of sulphur, through the production of cysteine and its used in the antioxidant glutathione pathway, also tended to differentiate the strains (**Figure 8**). The levels of sulphate in both T73 and BMV58 strains started relatively high and declined during early growth, but then they began to increase in the later time points. Both natural isolates strains, CR85 and YPS128, did not show this pattern, the former not changing, and the latter decreasing in sulphate over the whole time course. BMV58 strain started with the lowest levels of cysteine and glutathione, but it recovered similar levels to the other strains towards the end of the fermentation. The *S. cerevisiae* wine yeast T73 also was active in the synthesis of cysteine and glutathione. On the contrary, CR85 and YPS128 strains showed relatively flat levels of glutathione and their derivatives. Taurine biosynthesis, which is derived from cysteine, occurs only at very

low levels in plants and fungi. In our conditions, its pattern was quite different between the strains. Regarding the two *S. cerevisiae* strains, T73 started with undetectable levels of taurine and then increased at the end, while YPS128 started with much higher levels and then declined. It is not clear if taurine occurs in high enough amounts to affect wine properties, but many sulphur containing compounds have flavour properties (usually negative).

Differences in aroma production

Ten aroma compounds including fusel alcohols, acetate esters and ethyl esters were quantified along the fermentation process. The evolution of their extracellular concentrations across time was integrated into a heat map (**Figure 9, panel A**) and a principal component analysis was used to segregate the aroma profile of the final wines by strains (**Figure 9, panel B; Table S1**). Also, the reactions leading to aromas formation, including the intracellular amount of their precursor when detected, were depicted in **panel C** of **Figure 9**. At 12ºC, the natural *S. cerevisiae* YPS128 strain produced very few aroma compounds and segregated in the bottom right corner of the PCA plot (**Figure 9**, **panel B**). Cryotolerant strains produced more ethyl acetate than both *S. cerevisiae*, which was in accordance with the higher intracellular levels of acetyl-CoA found for CR85 and BMV58 (**Figure 4**, **Figure 7**). Strain BMV58 produced the largest amount of fusel alcohols and their acetate esters, notably 2-phenylethanol, isoamyl alcohol, isobutanol, 2-phenylethyl acetate, isoamyl acetate, and isobutyl acetate. On the contrary, T73 strain mainly produced ethyl esters (ethyl hexanoate, ethyl octanoate, and ethyl decanoate). Finally, the CR85 strain had an intermediate position,

producing higher levels of isobutanol, isobutyl acetate, and isoamyl alcohol than T73 and similar levels of ethyl decanoate. The previous results were in accordance with the higher intracellular levels of phenylpropanoids stated above in BMV58 (**Figure 7**) as well as with the higher intracellular amounts of alpha ketoisovalerate and alpha-keto isocaproate detected in BMV58 and CR85 strains (**Figure 9, panel C**). Also, in T73 strain which produced more ethyl esters, the intracellular levels of hexanoate and octanoate were higher if compared to BMV58 strain. Nevertheless, while in CR85 strain the intracellular amount of decanoate was in accordance with the extracellular levels of ethyldecanoate, surprisingly in T73 strain it was lower than in BMV58 strain.

Discussion

Global fermentation performances comparison between 12ºC and 25ºC

We recently performed a metabolomic comparison in a similar way with strains T73, BMV58, and CR85 at 25ºC (Minebois *et al.*, 2020). At 12ºC and 25ºC, most of the physiological and metabolic changes among strains occurred during the transition between the growth phase and the stationary phase. When comparing the global fermentation performances at both temperatures, no significant differences were observed in the ethanol yields (g of ethanol produced/ g sugar consumed) for the three strains, but were observed for the yield of various fermentative by-products and the biomass production. The *S. cerevisiae* strain T73 was the most negatively affected by low temperature. Its biomass production decreased and the yields of acetate and 2,3 butanediol increased. On the contrary, the CR85 strain performed much better at low temperature. We reported the absence of residual sugar (dry wine) at 12ºC in the CR85

fermentation, and we observed a significant decrease in the yields of acetate and lactate (data not shown) and a significant increase in erythritol yield. The last results pointed out the better adaptation of CR85 strain to low temperature. In BMV8 the yields of glycerol and lactate increased at 12ºC, while the yield of erythritol decreased. Interestingly, in CR85 strain, we observed that the intracellular levels of glycerol precursors, glycerol-3-phosphate and DHAP, were lower than those of BMV58 strain, as well as those of both *S. cerevisiae* strains which produced less glycerol. Consequently, only a higher catalytic property of the enzymes involved in the glycerol pathway of the CR85 strain could explain such intracellular amounts of the glycerol precursors. This meets with the described properties of the *S. kudriavzevii* Gpd1p enzyme encountered by Oliveira *et al.* (2014) but also with the adaptive evolution detected in the FBA1 gene of CR85, which is involved in the synthesis of dihydroxyacetone phosphate, the precursor of the glycerol synthesis (Macías *et al.*, 2019).

Regarding aroma production, at 12ºC BMV58 strain excelled in higher alcohol (2-phenyl ethanol, isoamyl alcohol, and isobutanol) and acetate esters (isoamyl acetate and 2-phenylethyl acetate) production, whereas T73 and CR85 strains did so in ethyl esters synthesis (ethyl hexanoate and ethyl decanoate). Also, at 12ºC cryotolerant CR85 and BMV58 strains produced a higher amount of ethyl acetate compared to the same fermentation performed at 25ºC. At 25ºC, the production of higher alcohols and acetate esters by BMV58 strain was already remarkable, as was acetic acid synthesis carried out by CR85 (Minebois *et al.*, 2020). These results were in accordance with previous results

(Gamero *et al.*, 2013). In particular, it has been shown that the aromatic amino acid decarboxylase *ARO10*, and the acetyltransferase *ATF2* were up-regulated in a *S. uvarum* strain when fermented at 12ºC (Gamero *et al.*, 2014), which supported the higher levels of fusel alcohols, notably 2-phenyl ethanol, and acetate esters produced by BMV58 at 12ºC. Gamero *et al.* (2014) also observed that alcohol dehydrogenases *ALD4* and *ALD5* (involved in acetaldehyde conversion into acetate) were up-regulated in the *S. uvarum* strain at 12ºC. One possible explanation for the low acetate levels detected in BMV58 is that part of this metabolite is used for ethyl acetate production since BMV58, together with CR85 strain, produced the largest ethyl acetate amount at 12ºC.

Anthranilate accumulation in S. kudriavzevii

In a metabolomic comparison performed at 12ºC, López-Malo et al. (2013) demonstrated that the CR85 strain was characterized by a high activity of the NAD^+ *de Novo* pathway. As evidence, most of the intermediates of this pathway, including tryptophan, nicotinate, nicotinamide ribonucleotide, or nicotinate ribonucleoside were present in higher amounts in the CR85 strain in comparison with the *S. cerevisiae* wine strain (QA23) used as control. Intriguingly, we observed that anthranilate, an upstream compound of the NAD^+ *de Novo* pathway and a precursor of tryptophan was highly accumulated (>150 fold) by the CR85 strain. Nevertheless, this did not correlate to tryptophan either its downstream catabolite kynurenate. The reason for such anthranilate accumulation might be found in the characteristics of the enzymes involved in this pathway. Indeed, while the conversion of anthranilate to L-tryptophan can occur anaerobically, three reactions involved in the *de Novo* pathway from L-tryptophan to

NAD^+ require oxygen. Notably, the 2,3 dioxygenase (Bna2p), the kynurenine 3-mono oxygenase (Bna4p), and the 3-hydroxyanthranilic acid dioxygenase (Bna1p) involved in the first, third and fifth steps from L-tryptophan respectively are oxygen-dependent (Panozzo *et al.*, 2002). In our study, anaerobic conditions were self-generated inside the bioreactors, but dissolved oxygen was already depleted at the time of the first intracellular sampling point (GP). On the contrary, López-Malo *et al.* (2013) used chemostat steady-state cultures, and it is not mentioned if fermenters were fed with a deoxygenized medium. Because it is not clear if anaerobic conditions were imposed in the work of López-Malo et al. (2013), it is likely that the higher activity of the *de Novo* NAD^+ pathway identified in the CR85 strain was allowed by the presence of dissolved oxygen in the medium. A very similar phenomenon exists in yeasts with squalene. The initial steps of sterol synthesis do not require oxygen and are responsible for the accumulation of squalene under anaerobic conditions (Daum *et al.*, 1998; Rosenfeld and Beauvoit, 2003). In our study, we could then expect that CR85 strain accumulated anthranilate as an attempt to fulfill its NAD^+ requirements. The couple NAD^+/NADH is a conserved moiety that can serve as a marker of the cellular redox status (Bakker *et al.*, 2001). Since alcoholic fermentation is redox neutral, under anaerobic conditions, other organic molecules such as glycerol have to act as proton acceptors. This correlates with the observation that, with the *S. uvarum* strain, CR85 strain is characterized by high glycerol yield. Regrettably, we had no information of the *de Novo* NAD^+ pathway in CR85 at 25ºC due to the lower number of metabolites that could be quantified with the GC/MS procedure we used for intracellular samples (Minebois *et al.*, 2020). Thus

further investigation is required to answer whether the CR85 strain also struggles to meet NAD+ levels via *de Novo* NAD^+ pathway at high temperature.

Higher pentose phosphate and chorismate pathways activity in BMV58 strain

In a previous study at 25ºC, we already reported the concomitant synthesis of erythritol, 2-phenyl ethanol, and 2-phenylethyl acetate following the onset of nitrogen starvation and the significantly higher yields for these metabolites in two *S. uvarum* strains, namely BMV58 and CECT12600 (Minebois *et al.*, 2020). These results led us to suggest that both strains were metabolically more active than T73 strain through the pentose phosphate and the chorismate pathways when passing from growth phase to the stationary phase. Indeed, both pathways have in common erythrose-4-phosphate. On the one hand, erythrose-4-phosphate is the precursor for erythritol synthesis (Moon *et al.*, 2010). Moreover, it is also an upstream precursor of the chorismate pathway whose downstream metabolites can be converted through the Ehrlich pathway into 2-phenylethanol and 2-phenylethyl acetate among others (Braus, 1991; Hazelwood *et al.*, 2008). In this study, the higher intracellular levels found for sugar precursors of the pentose phosphate pathway (xylulose and ribulose), erythritol, and the various aromatic precursors (3-dehydroquinate, 3-dehydro-shikimate, and shikimate) were clear evidence that this higher activity was maintained at low temperature in BMV58 strain. Also, these results were in accordance with a similar observation made by López-Malo *et al.* (2013) in chemostat culture. However, because the intracellular levels of the aforementioned metabolites were not quantified absolutely at 12ºC either at 25ºC, we

could not ascertain how much this activity is affected by low temperature in the *S. uvarum* strain.

Acetate and lipid metabolism in BMV58 strain

At 12°C, CR85 and BMV58 strains had lower acetate yields than the T73 strain. Also, the *S. cerevisiae* wine strain T73 produced more acetate at 12ºC when compared to the same fermentation performed at 25°C (Minebois *et al.*, 2020). The above results pointed out the better fermentative quality of both strains of *S. uvarum* and *S. kudriavzevii* at low fermentation temperature. Moreover, the dynamic approach used in our studies enabled us again to suggest a possible metabolism of "production-consumption" of acetate in the *S. uvarum* BMV58 strain at 12ºC. At 25ºC, this metabolomic trait was already observed in two *S. uvarum* strains, including BMV58, and occurs when cells are starved of nitrogen and in the absence of oxygen (Minebois *et al.*, 2020). Thus, these results suggest that this metabolic trait of BMV58 does not depend on temperature. But whether this mechanism requires strict anaerobic conditions or can occur under aerobic or limited aerobic conditions in the BMV58 strains has to be investigated. From an industrial point of view, it is relevant since it could help winemakers to reduce the volatile acidity of wines fermented at low or high temperature. Recently, the selection of yeast strains with the ability to consume acetate has already been explored for the deacidification of acidic wines (Vilela-Moura *et al.*, 2008, 2010, 2011). However, in the latter studies deacidification by both *S. cerevisiae* strains, namely S29 and S26, relies on their ability to consume acetate in the presence of

glucose and under limited-aerobic or aerobic conditions, i.e. on their ability to respire acetate even under glucose repression.

To explain this specific acetate metabolism in the *S. uvarum* BMV58 strain, we already suggested that acetate could be assimilated in the lipid-producing pathways at 25ºC (Minebois *et al.*, 2020). Although the assimilation mechanisms are not clear, other authors have suggested that acetate could be assimilated for such purpose (Ribéreau-Gayon *et al.*, 2006). Cadière *et al.* (2011) notably shown that the evolved strain ECA5 with higher pentose phosphate pathway activity tended to reduce acetate levels, hypothesizing greater lipid synthesis. At 12ºC, our intracellular data set revealed that the majority of high magnitude metabolic changes occurred for the four strains between the first (GP) and the second (EGP) intracellular sampling point were related to lipid metabolites. We reported that the CR85 and BMV58 strains had higher intracellular levels of acetyl-CoA. Also, the precursors of acetyl-CoA, pantothenate and CoA, were found in higher amount between GP and EGP in BMV58. In accordance with a higher acetyl-CoA requirement for lipids biosynthesis, the short chain fatty acids butanoate (4:0) and 3-methyl-butanoate (6:0), as well as the medium chain fatty acid myristate (14:0) were highly accumulated between GP and EGP in BMV58 and their intracellular levels remained higher until MSP. Moreover, octanoylcarnitine, a medium chain saturated fatty acyl-L-carnitine compound was only detected in BMV58. The presence of octanoylcarnitine only in the BMV58 strain remained unclear. However, in accordance with the results obtained by Redón *et al.* (2011) and the levels of butanoate and 3-methyl-butanoate observed in BMV58, we suggest that the BMV58 strain may

have favoured the synthesis of short and medium chain fatty acid as an adaptation mechanism to low fermentation temperature. Concordant with this, ethyl hexanoate, ethyl octanoate, and ethyl hexanoate aromas were barely detected in the *S. uvarum* fermentation when compared with T73 and CR85. Also, it is possible, that this medium chain fatty acid could enter into the specific mitochondrial membrane composition of the BMV58 strain.

In summary, this global metabolic profiling study gave us some new insights into the low fermentation temperature metabolism of strains of *S. cerevisiae*, *S. uvarum*, and *S. kudriavzevii*. The high resolution of the Metabolon HD4 platform (Durham, NC, USA) enabled us to accurately snapshot the intracellular levels of a large number of metabolites at four stages of the fermentation. Combining data of the intra- and extracellular metabolomes, we could reconstruct some relevant yeast pathways with their upstream and downstream metabolites. We already performed a similar metabolic profiling of strains T73, CR85, and BMV58 at 25ºC, but not with as much intracellular metabolome details. This made impossible a complete comparison between the 12ºC and the 25ºC metabolic data. Consequently, we could not ascertain whether the changes presented above in the metabolism of these strains were due to low temperature. However, up to a point we succeeded in shading between inherent strain difference and temperature-dependent strain difference. For instance, the higher pentose phosphate and chorismate pathways activity, as well as the "production-consumption" profile of acetate observed in BMV58 at 12ºC and 25ºC, suggested it is inherent to this strain. This work can have practical implications, taking advantage of the specific metabolic

properties and pathways identified in our set of *S. cerevisiae*, *S. kudriavzevii* and *S. uvarum* strains. From an industrial outlook, such knowledge is relevant to develop better metabolic engineering or hybridization strategies using cryotolerant strains of *S. uvarum* and *S. kudriavzevii*.

Experimental procedures

Yeast strains

Four strains from three different *Saccharomyces* species were used in this study. The commercial strain, T73 (Lalvin T73 from Lallemand, Montreal) originally isolated from wine in Alicante, Spain (Querol *et al.*, 1992) was used as our winemaking *S. cerevisiae* representative. We also included YPS128, isolated from Pennsylvania woodlands (Sniegowski *et al.*, 2002) as a representative of a wild *S. cerevisiae* strain. The commercial strain, BMV58, selected in our laboratory and commercialized for winemaking (Velluto BMV58 from Lallemand, Montreal) was used as a representative of *S. uvarum*. Finally, for *S. kudriavzevii*, we choose strain CR85, a wild isolate from oak tree bark identified by Lopes et al. (2010). Cryogenically preserved (-80ºC) strains were cultured and maintained on GPY plates (2% glucose, 2% agar, 0.5% peptone, 0.5% yeast extract) and stored at 4ºC.

Microvinification experiments

Bioreactors were inoculated at OD_{600} 0.1 (approximately 1 x 10^6 cells/ml) from starter cultures. Starter cultures were prepared by growing cells in an Erlenmeyer flask

containing 25 ml of GPY liquid medium (2% glucose, 0.5% peptone, 0.5% yeast extract) at 12°C and during 48 hours in an agitated incubator (Selecta, Barcelona, Spain) under aerobic conditions. We used a natural white must of Merseguera grapes variety collected in Titaguas (Spain) for the microvinification assays. Before its use, must was clarified by sedimentation for 24 h at 4°C and dimethyl dicarbonate (DMDC) at 1 $ml.L^{-1}$ added for sterilization purposes as described elsewhere (Peris *et al.*, 2016). Before fermentation, the fermentable sugar level was corrected as performed in most European countries by adding 47 g/l of chemically pure sucrose (AppliChem Panreac, Darmstadt, Germany) to reach a probable alcoholic grade of 12.5%. To avoid any stuck or sluggish fermentations, nitrogen content was adjusted by adding a nitrogen supplement, which consisted of 0.2 g/l of ammonium sulphate and 0.1 mg/l of thiamine hydrochloride (Sigma-Aldrich, Barcelona, Spain). All the fermentations were carried out in independent biological triplicates by using 470 ml of must in sterile 500 ml laboratory bioreactors (MiniBio, Applikon, the Netherlands). Data were integrated into the MyControl and BioExpert software (Applikon, The Netherlands). The evolution of the fermentation was followed by using different probes and detectors measuring temperature, pH, dissolved O_2 (AppliSens, Applikon, The Netherlands), and the proportion of carbon dioxide in the outgoing gas flow (Multi-Gas Monitors INNOVA 1316, LumaSense Technologies). Fermentations were monitored by measuring the residual sugar content by HPLC (see details below) until constant values were reached, considered to be the end of the fermentation.

Sampling

Bioreactors were sampled for extra- and intracellular metabolites profiling ensuring that total sampling volume remained below 10% of the total working volume. Approximately 3 ml of supernatant collected in ten time points distributed from the beginning to the end of the fermentation were used for extracellular metabolite quantification. For intracellular metabolites, a specific protocol was applied in four sampling points which were determined in function of growth curve value and time cultivation. The growth curve was calculated as $G(t) = \ln[OD_{600}(t)/OD_{600}(t_0)]$ and fitted to the Gompertz equation where A represents the maximum population level (details of the Gompertz equation are presented below). Intracellular samples were taken so that $G(t_1) = 0.75A$ (growth phase or GP), $G(t_2) = A$ (end of growth phase or EGP), $G(t_3=t_2+50/90h) = A$ (early stationary phase or ESP) and $G(t_4=t_3+70h) = A$ (mid-stationary phase or MSP). When the set-point was reached, a sample volume corresponding to approximately 30 OD_{600} of cells was rapidly harvested from the bioreactor and transferred to a 15 ml polypropylene tube. The tube was gently centrifuged at 750 x g for 3 min to pellet cells. The supernatant was removed and discarded all but ~0.75 ml. Cell pellets were softly re-suspended, transferred to a 2.0 ml polypropylene tube, and centrifuged in the same conditions. Then, the supernatant was carefully removed using micropipette tips to ensure a dry pellet for freezing, the tube was then flash-frozen in liquid nitrogen, and stored at -80 ºC until shipment to the HD4 platform of Metabolon, Inc. (Durham, NC, USA) for extraction and analysis.

Intracellular metabolites extraction and quantification

Samples were prepared using the automated MicroLab STAR® system from Hamilton Company. Several recovery standards were added before the first step in the extraction process for QC purposes. Samples were extracted with methanol under vigorous shaking for 2 min to precipitate protein and dissociate small molecules bound to protein or trapped in the precipitated protein matrix, followed by centrifugation to recover chemically diverse metabolites. The resulting extract was divided into five fractions: two for analysis by two separate reverse phase (RP)/UPLC-MS/MS methods using positive ion mode electrospray ionization (ESI), one for analysis by RP/UPLC-MS/MS using negative ion mode ESI, one for analysis by HILIC/UPLC-MS/MS using negative ion mode ESI, and one reserved for backup. Samples were placed briefly on a TurboVap® (Zymark) to remove the organic solvent. The sample extracts were stored overnight under nitrogen before preparation for analysis by Ultrahigh Performance Liquid Chromatography-Tandem Mass Spectroscopy (UPLC-MS/MS) as described in the supplementary material.

Extracellular metabolite quantification

Sugars (glucose, fructose), fermentative by-products (glycerol, ethanol, 2,3 butanediol, and erythritol) and organic acids were respectively determined by HPLC (Thermo Fisher Scientific, Waltham, MA) using a refraction index detector and UV/VIS (210 nm) detector equipped with a HyperREZ^{TM} XP Carbohydrate H+ 8 mm column (Thermo Fisher Scientific, Waltham, MA) and HyperREZ^{TM} XP Carbohydrate Guard (Thermo Fisher Scientific, Waltham, MA). The analysis conditions were: eluent, 1.5 mM of H_2SO_4; 0.6 ml.min^{-1} flux, and oven temperature of 50°C. For sucrose

determination, the same HPLC was equipped with a Hi-Plex Pb, 300 x 7.7 mm column (Agilent Technologies, CA, USA), and peaks quantified by the RI detector. The analysis conditions were: eluent, Milli-Q water; 0.6 ml.min-1 flux, and oven temperature of 50°C. The retention times of the eluted peaks were compared to those of commercial analytical standards (Sigma-Aldrich, Madrid, Spain). Concentration of the target compounds, in g/l, were quantified by the calibration graphs (R2 value > 0.99) of the standards that were previously obtained from a linear curve fit of the peak areas using standards mixtures.

Determination of yeast assimilable nitrogen (YAN) in the form of amino-acids and ammonia was carried out using the same protocol as Su *et al*. (2020). For derivatization, 400 µl of the sample was mixed with 430 µl borate buffer (1 M, pH 10.2), 300 µl absolute methanol and 12 µl of diethyl ethoxymethylenemalonate (DEEMM), and ultra-sonicated for 30 min at 20ºC. After ultra-sonicating, the sample was warmed up at 80ºC for 2 hours to allow the complete degradation of excess DEEMM, and once derivatization finished the sample was filtered with 0.22 µm filter. The chromatographic instrument consisted in a UPLC Dionex Ultimate 3000 (Thermo Fisher Scientific, Waltham, MA) equipped with a Kinetex 2.6u C18 100A column (Phenomenex, Torrance, CA, USA) and Accucore C18 10 x 4.6 mm 2.6 um Defender guards (Thermo Fisher Scientific, Waltham, MA). Amino-acids and ammonia in the samples were identified and quantified according to the retention times, UV-vis spectral characteristics and calibration curves (R2 value > 0.99) of the derivatives of the

corresponding standards. Amino acid standard (ref AAS18), asparagine and glutamine purchased from Sigma-Aldrich were used for calibration.

Volatile compounds extraction and quantification

Volatile compounds extraction and gas chromatography were performed following the protocol of Stribny et al. (2015). 1.5 mL of the supernatant was transferred to 15-mL vials with 0.35 g of NaCl. 20 µl volume of 2-heptanone (0.005 %) was added as an internal standard. Higher alcohols and esters were analyzed by the headspace solid-phase microextraction (HS-SPME) technique with 100-µm polydimethylsiloxane (PDMS) fiber (Supelco, Sigma-Aldrich, Madrid, Spain). Solutions were maintained for 2 h at 20°C to establish the headspace-liquid equilibrium. The fiber was inserted into the headspace through a vial septum and was held for 7 min. The fiber was then inserted into the gas chromatograph inlet port for 4 min at 220°C with helium flow (1 mL/min) to desorb analytes. A Thermo Science TRACE GC Ultra gas chromatograph with a flame ionization detector (FID) was used, equipped with an HP INNOWax 30 m × 0.25 m capillary column coated with a 0.25-m layer of cross-linked polyethylene glycol (Agilent Technologies, Valencia, Spain). The oven temperature program was: 5 min at 35°C, 2°C/min to 150°C, 20°C/ min to 250°C and 2 min at 250°C. The detector temperature was kept constant at 280°C. Volatile compounds were identified by the retention time for reference compounds. Quantification of the volatile compounds was determined using the calibration graphs of the corresponding standard volatile compounds.

Biomass and physiological parameters determination

Biomass and physiological parameters - OD_{600}, dry weight (DW), and average cell diameter (ACD) - were determined in every sampling point providing that cell sample was sufficient to perform the corresponding measure. For DW determination, 2 ml of a fresh sample placed in a pre-weighed Eppendorf tube were centrifuged at maximum speed (13.400 rpm) in a MiniSpin centrifuge (Eppendorf, Spain) for 5 minutes. The supernatant was carefully removed with a pipette, the pellet washed twice with 70 % (v/v) ethanol and centrifuged in the same conditions. After washing, the aqueous supernatant was carefully removed and tube stored at 65ºC for 72h until dryness. DW was obtained by measuring the mass weight difference of tubes with a BP121S analytical balance (Sartorius, Gottingen, Germany). OD_{600} was measured at each sampling point using a diluted volume of sample and a Biophotometer spectrophotometer (Eppendorf, Hamburg, Germany). For ACD determination, a volume of cell sample was diluted into phosphate-buffered saline solution and cell diameter measured using a Scepter Handled Automated Cell Counter equipped with a 40 µm sensor (Millipore, Billerica, USA).

Statistical analysis

To describe the temporal production of the main fermentative by-products (ethanol, glycerol, 2,3 butanediol, succinate, acetate, and erythritol), the consumption of YAN and the cell population, biological data were fitted to mathematical equations using non-linear regression and the GraphPad Prism 6.0 Software package (La Jolla,

CA, USA) to provide biological parameters. Best-fit parameters were determined minimizing the sum of squares of the difference between experimental data and the fitted model, and following the general recommendations of Motulsky and Christopoulos (2004). For each parameter, a 95% confidence interval was approximated by using the estimated predictions and standard errors. Conditions for which the confidence intervals do not intersect can be considered significantly different. The following mathematical equations were used:

- Gompertz decay function, previously described by Tronchoni et al. (2009). Function to fit: $Y(t) = Ymin+(Ymax-Ymin)*exp(-exp(r*(t-T50)))$. Where Ymin and Ymax are the minimum and maximum values (Y units), r the maximum consumption rate (h^{-1}) and T50 the time to reach ½Ymax (h).
- Modified Boltzman sigmoidal function, previously described by Motulsky and Christopoulos (2004). Function to fit: $Y(t) = Ymin+(Ymax-Ymin)/(1+exp(r*(T50-t)))$. Where Ymin and Ymax are the minimum and maximum values (Y units), r the maximum production rate (h^{-1}), and T50 the time to reach ½Ymax (h).
- Modified Gompertz function, used for cell growth curve and previously described by Zwietering et al. (1990). Function to fit: $G(t) = A*exp(-exp((((\mu_{max}*e)/A)*(\lambda-t))+1))$. Where G(t) is the cell population at time t (in this study calculated as $ln[OD_{600}(t)/OD_{600}(t_0)]$), A is the maximum population level (Y units), μ_{max} the maximum growth rate (h^{-1}) and λ the lag time (h) defined as the time axis intercept of the tangent through the inflection point.

- One phase exponential association, previously described by Motulsky and Christopoulos (2004). Function to fit: Y(t) = Ymin + (Ymax-Ymin)*(1-exp(-K*t)). Ymin and Ymax are the minimum and maximum values (Y units), and K the rate constant (h^{-1}).

For a general overview of growth, fermentative by-products production and nitrogen consumption trait data, a principal component analysis (PCA) was performed using the Statsoft Statistica 10 Package, with the following variables obtained from the above models: DW_{max} (maximum dry weight biomass), μ_{max} (maximum growth rate), λ (lag phase), r_{YAN} (maximum consumption rate of YAN), $T_{50}YAN$ (estimated time at which 50% of the total YAN content was consumed), g_{DW}/g_{YAN} (maximum biomass yield), r_{EtOH} (maximum production rate of ethanol), $EtOH_{max}$ (maximum ethanol concentration at the end of fermentation), r_{Gly} (maximum production rate of glycerol), Gly_{max} (maximum glycerol concentration at the end of fermentation), r_{But} (maximum production rate of 2,3 butanediol), But_{max} (maximum 2,3 butanediol concentration at the end of fermentation), r_{Ac} (maximum production rate of acetate), Ac_{max} (maximum acetate concentration at the end of fermentation), r_{Succ}(maximum production rate of succinate), $Succ_{max}$ (maximum succinate concentration at the end of fermentation), r_{Ery} (maximum production rate of erythritol) and Ery_{max} (maximum erythritol concentration at the end of fermentation). PCA plot of aroma compounds at the end of the fermentation was also obtained using the Statsoft Statistica 10 Package.

For intracellular samples, data were normalized for internal consistency by processing a constant amount of sample per volume of extraction solvent. Data were

scaled to the median value for each compound, and missing values (if any) were imputed with the minimum detected value for that compound. Statistical calculations and figures were performed and obtained using natural log-transformed scaled imputed data.

Acknowledgments

RM was supported by a FPI grant from the Ministerio de Economía y Competitividad (ref. BES-2016-078202). This work was supported by the Spanish government projects RTI2018-093744-B-C31 awarded to AQ.

References

Arroyo-López, F.N., Pérez-Torrado, R., Querol, A., and Barrio, E. (2010) Modulation of the glycerol and ethanol syntheses in the yeast *Saccharomyces kudriavzevii* differs from that exhibited by *Saccharomyces cerevisiae* and their hybrid. *Food Microbiol* **27**: 628–637.

Bakker, B.M., Overkamp, K.M., Van Maris, A.J.A., Kötter, P., Luttik, M.A.H., Van Dijken, J.P., and Pronk, J.T. (2001) Stoichiometry and compartmentation of

NADH metabolism in *Saccharomyces cerevisiae*. *FEMS Microbiol Rev* **25**: 15–37.

Belloch, C., Orlic, S., Barrio, E., and Querol, A. (2008) Fermentative stress adaptation of hybrids within the *Saccharomyces* sensu stricto complex. *Int J Food Microbiol* **122**: 188–195.

Beltran, G., Novo, M., Leberre, V., Sokol, S., Labourdette, D., Guillamon, J.M., et al. (2006) Integration of transcriptomic and metabolic analyses for understanding the global responses of low-temperature winemaking fermentations. *FEMS Yeast Res* **6**: 1167–1183.

Blateyron, L. and Sablayrolles, J.M. (2001) Stuck and slow fermentations in enology: Statistical study of causes and effectiveness of combined additions of oxygen and diammonium phosphate. *J Biosci Bioeng* **91**: 184–189.

Braus, G.H. (1991) Aromatic amino acid biosynthesis in the yeast *Saccharomyces cerevisiae*: A model system for the regulation of a eukaryotic biosynthetic pathway. *Microbiol Rev* **55**: 349–370.

Cadière, A., Ortiz-Julien, A., Camarasa, C., and Dequin, S. (2011) Evolutionary engineered *Saccharomyces cerevisiae* wine yeast strains with increased in vivo flux through the pentose phosphate pathway. *Metab Eng* **13**: 263–271.

Clement, T., Perez, M., Mouret, J.R., Sablayrolles, J.M., and Camarasa, C. (2011) Use of a continuous multistage bioreactor to mimic winemaking fermentation. *Int J Food Microbiol* **150**: 42–49.

Daum, G., Lees, N.D., Bard, M., and Dickson, R. (1998) Biochemistry, cell biology and molecular biology of lipids of *Saccharomyces cerevisiae*. *Yeast* **14**: 1471–1510.

Demuyter, C., Lollier, M., Legras, J.L., and Le Jeune, C. (2004) Predominance of *Saccharomyces uvarum* during spontaneous alcoholic fermentation, for three consecutive years, in an Alsatian winery. *J Appl Microbiol* **97**: 1140–1148.

Gamero, A., Belloch, C., Ibáñez, C., and Querol, A. (2014) Molecular analysis of the genes involved in aroma synthesis in the species *S. cerevisiae, S. kudriavzevii* and *S. bayanus* var. *uvarum* in winemaking conditions. *PLoS One* **9**: 1–10.

Gamero, A., Tronchoni, J., Querol, A., and Belloch, C. (2013) Production of aroma compounds by cryotolerant *Saccharomyces* species and hybrids at low and moderate fermentation temperatures. *J Appl Microbiol* **114**: 1405–1414.

García-Ríos, E., Querol, A., and Guillamón, J.M. (2016) iTRAQ-based proteome profiling of *Saccharomyces cerevisiae* and cryotolerant species *Saccharomyces uvarum* and *Saccharomyces kudriavzevii* during low-temperature wine fermentation. *J Proteomics* **146**: 70–79.

Hazelwood, L.A., Daran, J.-M., van Maris, A.J.A., Pronk, J.T., and Dickinson, J.R. (2008) The Ehrlich pathway for fusel alcohol production: a century of research on *Saccharomyces cerevisiae* metabolism. *Appl Environ Microbiol* **74**: 2259–66.

Lopes, C.A., Barrio, E., and Querol, A. (2010) Natural hybrids of *S. cerevisiae* × *S. kudriavzevii* share alleles with European wild populations of *Saccharomyces*

kudriavzevii. *FEMS Yeast Res* **10**: 412–421.

López-Malo, M., Querol, A., and Guillamon, J.M. (2013) Metabolomic Comparison of *Saccharomyces cerevisiae* and the Cryotolerant species *S. bayanus* var. *uvarum* and *S. kudriavzevii* during Wine Fermentation at Low Temperature. *PLoS One* **8**:.

Macías, L.G., Morard, M., Toft, C., and Barrio, E. (2019) Comparative genomics between *Saccharomyces kudriavzevii* and *S. cerevisiae* applied to identify mechanisms involved in adaptation. *Front Genet* **10**: 187.

Masneuf-Pomarède, I., Bely, M., Marullo, P., Lonvaud-Funel, A., and Dubourdieu, D. (2010) Reassessment of phenotypic traits for *Saccharomyces bayanus* var. *uvarum* wine yeast strains. *Int J Food Microbiol* **139**: 79–86.

Matallana, E. and Aranda, A. (2017) Biotechnological impact of stress response on wine yeast. *Lett Appl Microbiol* **64**: 103–110.

Minebois, R., Pérez-Torrado, R., and Querol, A. (2020) A time course metabolism comparison among *Saccharomyces cerevisiae*, *S. uvarum* and *S. kudriavzevii* species in wine fermentation. *Food Microbiol* **90**: 103484.

Molina, A.M., Swiegers, J.H., Varela, C., Pretorius, I.S., and Agosin, E. (2007) Influence of wine fermentation temperature on the synthesis of yeast-derived volatile aroma compounds. *Appl Microbiol Biotechnol* **77**: 675–687.

Moon, H.J., Jeya, M., Kim, I.W., and Lee, J.K. (2010) Biotechnological production of erythritol and its applications. *Appl Microbiol Biotechnol* **86**: 1017–1025.

Motulsky, H. and Christopoulos, A. (2004) Fitting Models to Biological Data Using Linear and Nonlinear Regression. A practical guide to curve fitting. In, *Fitting Models to Biological Data Using Linear and Nonlinear Regression*., pp. 160–165.

Naumov, G.I., Masneuf, I., Naumova, E.S., Aigle, M., and Dubourdieu, D. (2000) Association of *Saccharomyces bayanus* var. *uvarum* with some French wines: Genetic analysis of yeast populations. *Res Microbiol* **151**: 683–691.

Oliveira, B.M., Barrio, E., Querol, A., and Pérez-Torrado, R. (2014) Enhanced enzymatic activity of glycerol-3-phosphate dehydrogenase from the cryophilic *Saccharomyces kudriavzevii*. *PLoS One* **9**:.

Panozzo, C., Nawara, M., Suski, C., Kucharczyka, R., Skoneczny, M., Bécam, A.M., et al. (2002) Aerobic and anaerobic NAD+ metabolism in *Saccharomyces cerevisiae*. *FEBS Lett* **517**: 97–102.

Pérez-Torrado, R., Barrio, E., and Querol, A. (2018) Alternative yeasts for winemaking: *Saccharomyces* non-*cerevisiae* and its hybrids. *Crit Rev Food Sci Nutr* **58**: 1780–1790.

Peris, D., Pérez-Torrado, R., Hittinger, C.T., Barrio, E., and Querol, A. (2018) On the origins and industrial applications of *Saccharomyces cerevisiae* × *Saccharomyces kudriavzevii* hybrids. *Yeast* **35**: 51–69.

Peris, D., Pérez-Través, L., Belloch, C., and Querol, A. (2016) Enological characterization of Spanish *Saccharomyces kudriavzevii* strains, one of the closest

relatives to parental strains of winemaking and brewing *Saccharomyces cerevisiae* × *S. kudriavzevii* hybrids. *Food Microbiol* **53**: 31–40.

Querol, A., Huerta, T., Barrio, E., and Ramon, D. (1992) Dry Yeast Strain For Use in Fermentation of Alicante Wines: Selection and DNA Patterns. *J Food Sci* **57**: 183–185.

Redón, M., Guillamón, J.M., Mas, A., and Rozès, N. (2011) Effect of growth temperature on yeast lipid composition and alcoholic fermentation at low temperature. *Eur Food Res Technol* **232**: 517–527.

Ribéreau-Gayon, P., Dubourdieu, D., Donèche, B., and Lonvaud, A. (2006) Handbook of Enology: Volume 1, The Microbiology of Wine and Vinifications. *Handb Enol* **1**: 1–441.

Rosenfeld, E. and Beauvoit, B. (2003) Role of the non-respiratory pathways in the utilization of molecular oxygen by *Saccharomyces cerevisiae*. *Yeast* **20**: 1115–1144.

Sampaio, J.P. and Gonçalves, P. (2008) Natural populations of *Saccharomyces kudriavzevii* in Portugal are associated with Oak bark and are sympatric with *S. cerevisiae* and *S. paradoxus*. *Appl Environ Microbiol* **74**: 2144–2152.

Sniegowski, P.D., Dombrowski, P.G., and Fingerman, E. (2002) *Saccharomyces cerevisiae* and *Saccharomyces paradoxus* coexist in a natural woodland site in North America and display different levels of reproductive isolation from

European conspecifics. *FEMS Yeast Res* **1**: 299–306.

Stribny, J., Gamero, A., Pérez-Torrado, R., and Querol, A. (2015) *Saccharomyces kudriavzevii* and *Saccharomyces uvarum* differ from *Saccharomyces cerevisiae* during the production of aroma-active higher alcohols and acetate esters using their amino acidic precursors. *Int J Food Microbiol* **205**: 41–46.

Su, Y., Seguinot, P., Sanchez, I., Ortiz-Julien, A., Heras, J.M., Querol, A., et al. (2020) Nitrogen sources preferences of non-*Saccharomyces* yeasts to sustain growth and fermentation under winemaking conditions. *Food Microbiol* **85**:.

Tosi, E., Azzolini, M., Guzzo, F., and Zapparoli, G. (2009) Evidence of different fermentation behaviours of two indigenous strains of *Saccharomyces cerevisiae* and *Saccharomyces uvarum* isolated from Amarone wine. *J Appl Microbiol* **107**: 210–218.

Tronchoni, J., Gamero, A., Arroyo-López, F.N., Barrio, E., and Querol, A. (2009) Differences in the glucose and fructose consumption profiles in diverse *Saccharomyces* wine species and their hybrids during grape juice fermentation. *Int J Food Microbiol* **134**: 237–243.

Tronchoni, J., Medina, V., Guillamón, J.M., Querol, A., Pérez-Torrado, R. (2014). Transcriptomics of cryophilic *Saccharomyces kudriavzevii* reveals the key role of gene translation efficiency in cold stress adaptations. BMC Genomics. 15:432.

Varela, C., Sengler, F., Solomon, M., and Curtin, C. (2016) Volatile flavour profile of

reduced alcohol wines fermented with the non-conventional yeast species *Metschnikowia pulcherrima* and *Saccharomyces uvarum*. *Food Chem* **209**: 57–64.

Vilela-Moura, A., Schuller, D., Mendes-Faia, A., and Côrte-Real, M. (2010) Effects of acetic acid, ethanol, and SO2 on the removal of volatile acidity from acidic wines by two *Saccharomyces cerevisiae* commercial strains. *Appl Microbiol Biotechnol* **87**: 1317–1326.

Vilela-Moura, A., Schuller, D., Mendes-Faia, A., and Côrte-Real, M. (2008) Reduction of volatile acidity of wines by selected yeast strains. *Appl Microbiol Biotechnol* **80**: 881–890.

Vilela-Moura, A., Schuller, D., Mendes-Faia, A., Silva, R.D., Chaves, S.R., Sousa, M.J., and Côrte-Real, M. (2011) The impact of acetate metabolism on yeast fermentative performance and wine quality: Reduction of volatile acidity of grape musts and wines. *Appl Microbiol Biotechnol* **89**: 271–280.

Zwietering, M.H., Jongenburger, I., Rombouts, F.M., and Van't Riet, K. (1990) Modeling of the bacterial growth curve. *Appl Environ Microbiol* **56**: 1875–1881.

Figure legends

Figure 1

A) Overview of the fermentation kinetics of the four strains at 12ºC, with total sugar consumption expressed as percentage (black dashed line), yeast assimilable nitrogen

(YAN) content expressed as percentage (orange solid line), dissolved oxygen expressed as percentage (blue solid line), CO_2 exhaust concentration as percentage (black dashed line), cell population expressed as ln[OD600 (t) / OD600 (t0)] (grey solid line) with t0 the time of inoculation and time of intracellular samplings (red arrows). B) Detail of the evolution of the extracellular concentration of the three preferable nitrogen sources (ammonia, arginine, and glutamine) in yeasts and proline.

Figure 2

Average cell diameter (ACD) expressed in μm along the fermentation process. For each strain, the lag phase (λ), the growth phase and the stationary phase were indicated, as well as the timing of dissolved oxygen and YAN depletion. The values are displayed as mean and standard deviations from triplicate experiments.

Figure 3

Principal component analysis plot of the growth and by-products variables obtained for each strain after fitting our biological data to mathematical models (Supporting information in material and methods section). A total of 18 variables (6 growth and 12 by-products variables) which values are available in Table 1, were used for the PCA analysis.

Figure 4

A) Principal component analysis plot of the intracellular samples. On the left PCA plot, color circles indicate the segregation of triplicates by strains. Blue circle for BMV58 strain, pink circle for T73 strain, yellow circle for YPS128 strain and green circle for CR85 strain. On the right PCA plot, red circles indicate segregation of the triplicates by sampling time point, namely first intracellular sampling point or GP (1), second intracellular sampling point or EGP (2), third intracellular sampling point or ESP (3) and fourth intracellular sampling point or MSP (4).

B) Number of compounds which amount significantly changed ($p \leq 0.05$) in each pair-wise comparison of intracellular sampling points, and the direction of those changes. Grey bar indicate the total number of compounds that met the significant criteria, red bar the number of compounds that significantly increased and green bar the number of compounds that significantly decreased.

Figure 5

On panel A), list of the present or absent compounds detected among the four strains. On panel B), compounds with high magnitude change observed during growth among the four strains. For each strain, superscript italic letters indicate the magnitude (M) of the change between the first (GP) and the fourth sampling point (MSP) computed as M=exp[log scaled intensity(MSP) – log scaled intensity (GP)]. When the intracellular amount increased (M >1), the black letter was used. When decreased (M<1), the inverse of the magnitude (1/M) between GP and MSP was calculated and indicated in italic red letter. Highest changed in magnitude are indicated in bold.

Figure 6

Overview of the reactions involved in the CCM of yeasts under enological fermentative conditions, including the glycolysis pathway and the tricarboxylic acid (TCA) cycle. Dashed arrows indicate the uncomplete pathways. The intracellular amount of relevant intermediates of the CCM is presented for each strain. On intracellular graph, for each strain, superscript italic letters indicate the magnitude (M) of the change between the first (GP) and the fourth sampling point (MSP) computed as M=exp[log scaled intensity(MSP) – log scaled intensity (GP)]. When the intracellular amount increased (M >1), the black letter was used. When decreased (M<1), the inverse of the magnitude (1/M) between GP and MSP was calculated and indicated in italic red letter. For CoA and Pantothenate compounds, the magnitude between the second and fourth intracellular point is also presented in purple. Highest changed in magnitude are indicated in bold. Fitted extracellular concentration (supporting information in material and methods) and yield (g product/g sugar consumed) of the related CCM by products, including glycerol, 2,3 butanediol, ethanol and acetate are also included. Superscript letters on yield graph indicate the significant homogeneous groups obtained by one-way ANOVA analysis (Tukey test, n = 3, p-value <0.05). Circles on the fitted curves represent the four intracellular sampling points. Abbreviations: DHAP (dihydroxyacetone phosphate), GA-3-P (Glyceraldehyde-3-phosphate), PEP (phosphoenolpyruvate), α-Ac.Lact (alpha-acetolactate), α-KIV (alpha-ketoisovalerate), α-KIC (alpha-ketoisocaproate), α-KG (apha-ketoglutarate).

Figure 7

Overview of the reactions involved in the pentose phosphate pathway (PPP) and the chorismate pathway. Dashed arrows indicate the uncomplete pathways. The intracellular amount of relevant intermediates of the PPP and the chorismate pathway is presented for each strain. On intracellular graph, for each strain, superscript italic letters indicate the magnitude (M) of the change between the first (GP) and the fourth sampling point (MSP) computed as M=exp[log scaled intensity(MSP) – log scaled intensity (GP)]. When the intracellular amount increased (M >1), black letter was used. When decreased (M<1), the inverse of the magnitude (1/M) between GP and MSP was calculated and indicated in italic red letter. Highest changed in magnitude are indicated in bold. Fitted extracellular concentration (supporting information in material and methods) and yield (g product/g sugar consumed) of one of the related PPP by product, namely erythritol is also included. Superscript letters on yield graph indicate the significant homogeneous groups obtained by one-way ANOVA analysis (Tukey test, n = 3, p-value <0.05). Circles on the fitted curves represent the four intracellular sampling points. Abbreviations: 6P-Glu-δ-lac (6-phospho D-glucono-1,5-lactone), Rib-5-P (Ribulose-5-phosphate), Xyl-5-P (Xylulose-5-Phosphate), Ery-4-P (D-erythrose-4-phosphate), PEP (phosphoenolpyruvate), DAH-7-P (3-deoxy-D-arabino-heptulosonate 7-phosphate), Glu-6-P (Glucose-6-phosphate).

Figure 8

Overview of the glutathione biosynthesis pathway. Dashed arrows indicate the uncomplete pathways. On intracellular graph, for each strain, superscript italic letters indicate the magnitude (M) of the change between the first (GP) and the fourth sampling point (MSP) computed as M=exp[log scaled intensity(MSP) – log scaled intensity (GP)]. When the intracellular amount increased (M >1), black letter was used. When decreased (M<1), the inverse of the magnitude (1/M) between GP and MSP was calculated and indicated in italic red letter. Highest changed in magnitude are indicated in bold. Abbreviations: GSH (L-γ-glutamyl-L-cysteinylglycine), GSSG (glutathione oxidized).

Figure 9

A) Heat map of the extracellular concentrations of the ten aroma compounds quantified in this study, including fusel alcohols (isobutanol, isoamyl alcohol and 2-phenylethanol), acetate esters (isobutyl acetate, isoamyl acetate and 2-phenylethyl acetate) and ethyl esters (ethyl hexanoate, ethyl octanoate and ethyl decanoate). On the time axis of the heat map, red letters indicate the intracellular sampling points (GP, EGP, ESP, and MSP). B) PCA plots performed with the concentrations of aroma compounds at the end of the fermentation. C) Aroma compounds pathways with the intracellular amount of some precursors. On intracellular graph, for each strain, superscript italic letters indicate the magnitude (M) of the change between the first (GP) and the fourth sampling point (MSP) computed as M=exp[log scaled intensity(MSP) – log scaled intensity (GP)]. When the intracellular amount increased (M >1), black letter

was used. When decreased (M<1), the inverse of the magnitude (1/M) between GP and MSP was calculated and indicated in italic red letter. Highest changed in magnitude are indicated in bold. For 2-phenyl-ethanol and 2-phenylethyl acetate pathway, report to Figure 7. Abbreviations: α-KIV (alpha-ketoisovalerate) and α-KIC (alpha-ketoisocaproate).

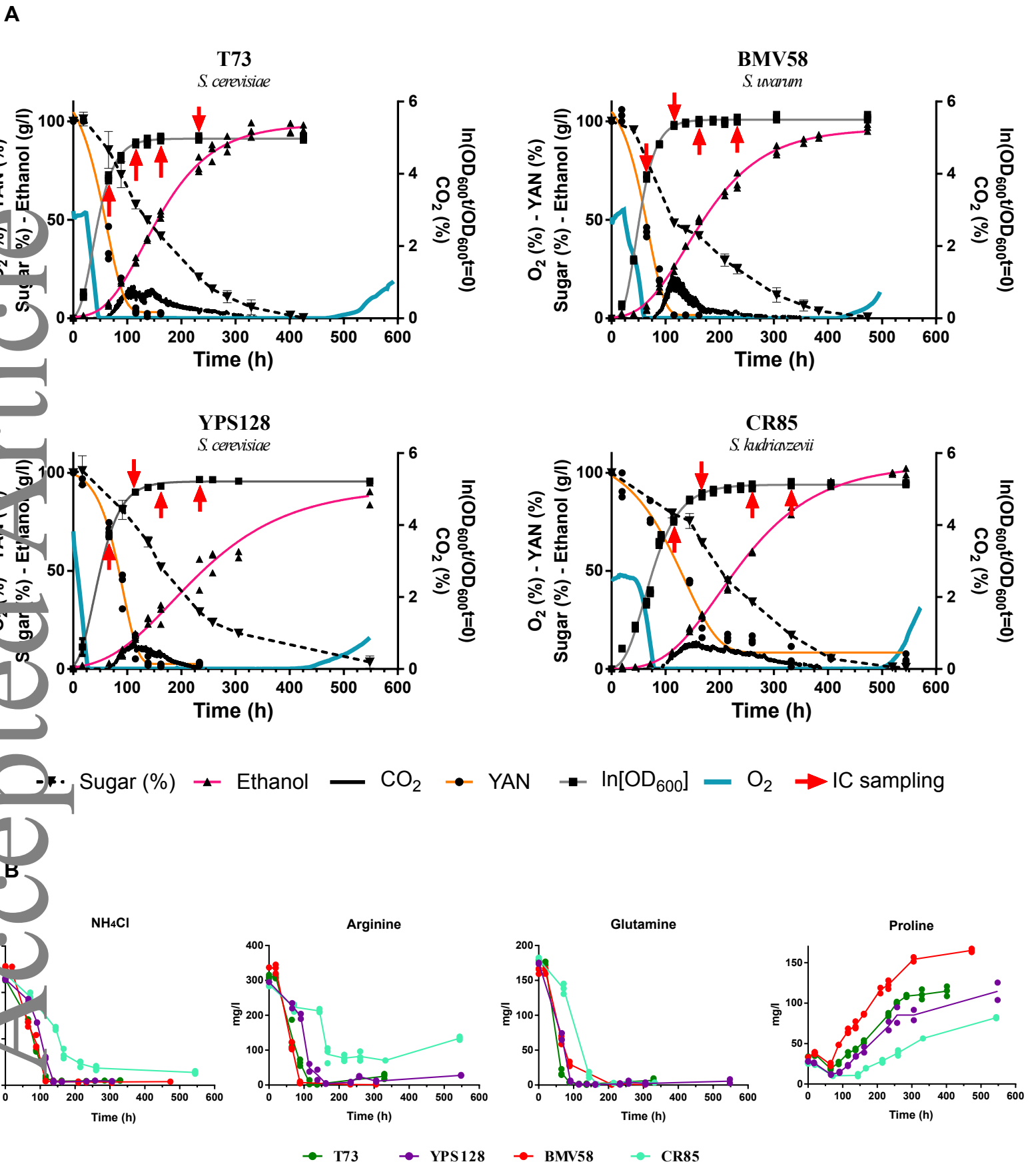

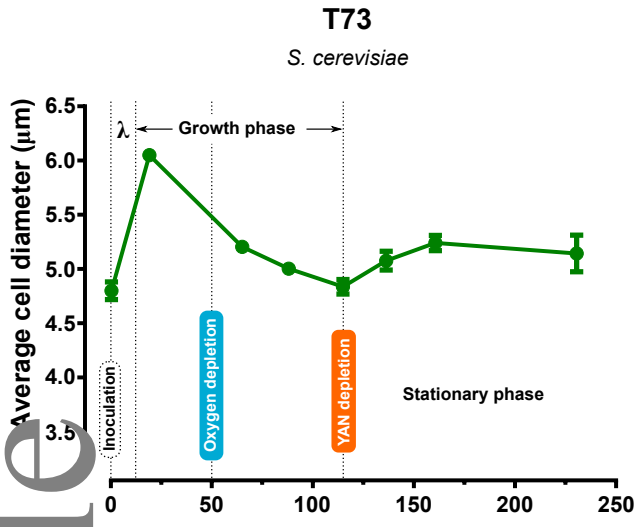

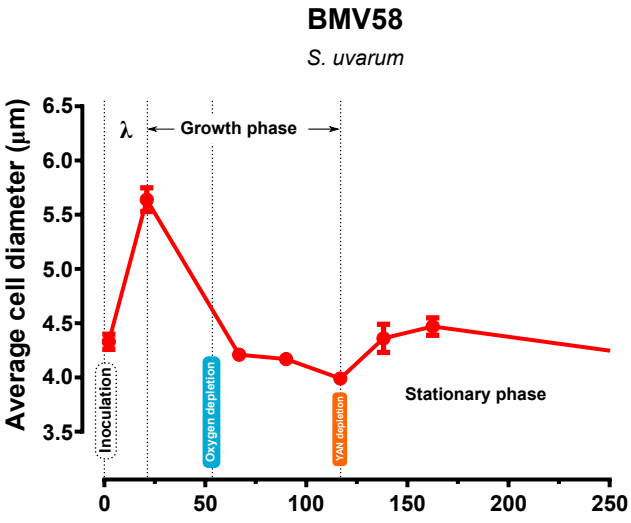

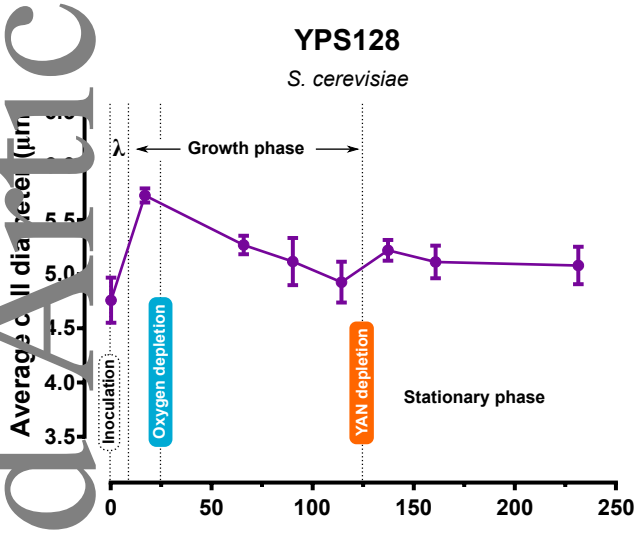

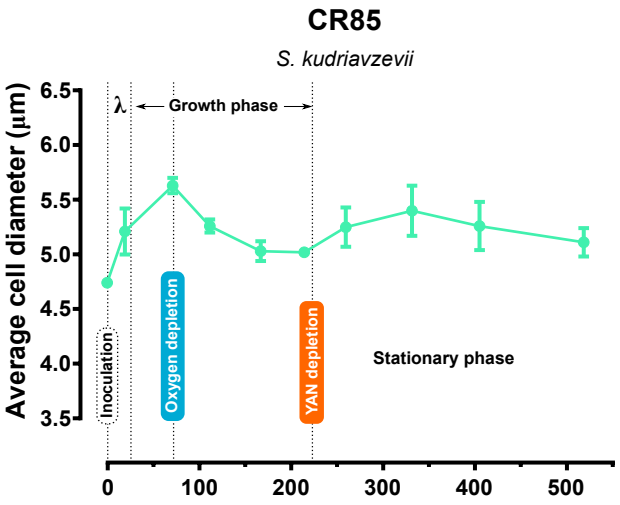

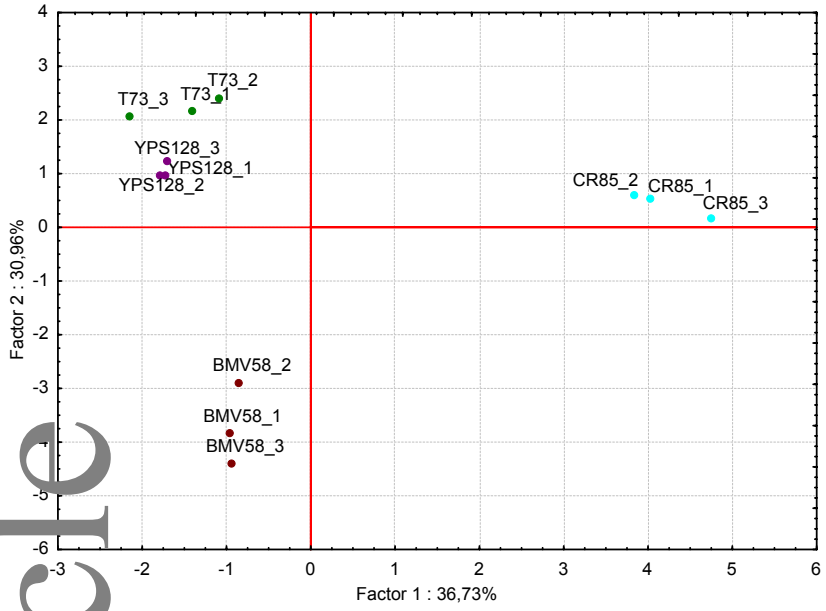

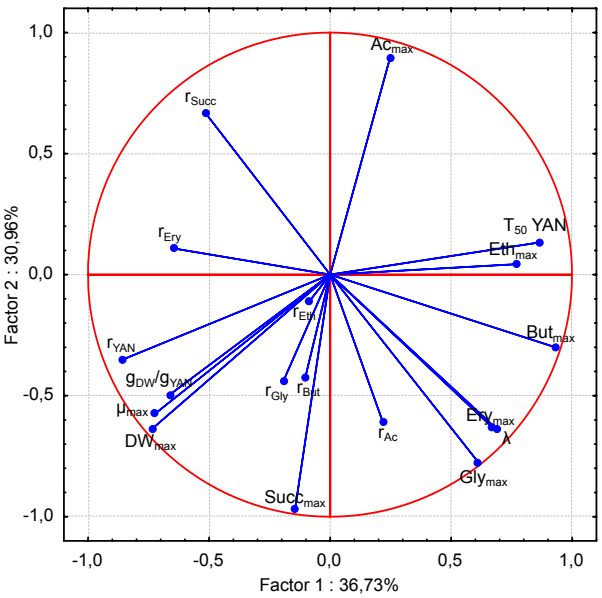

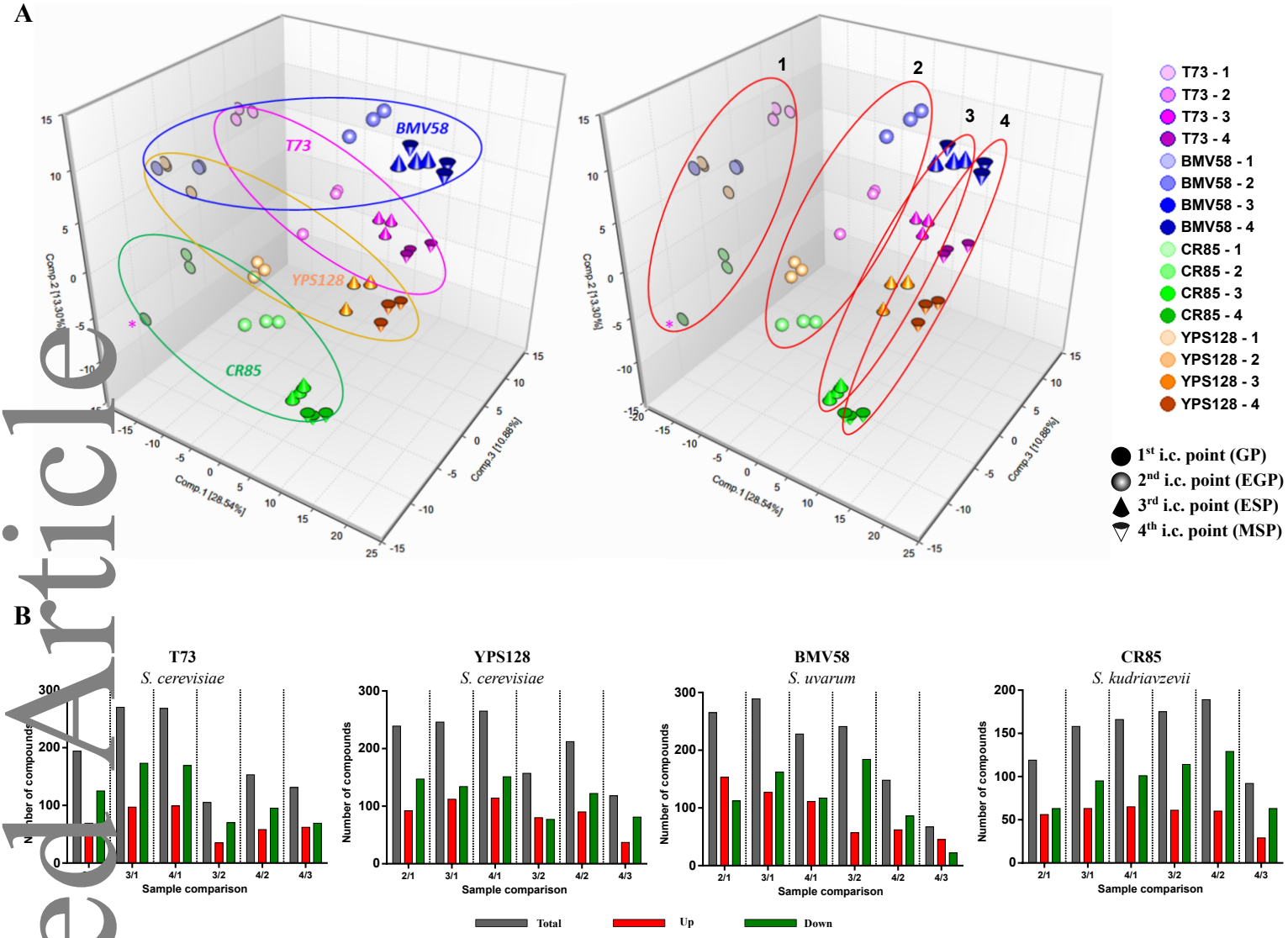

A

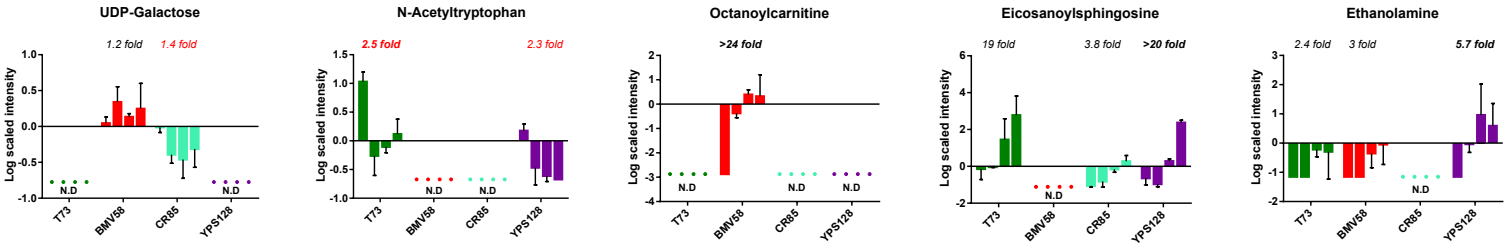

B

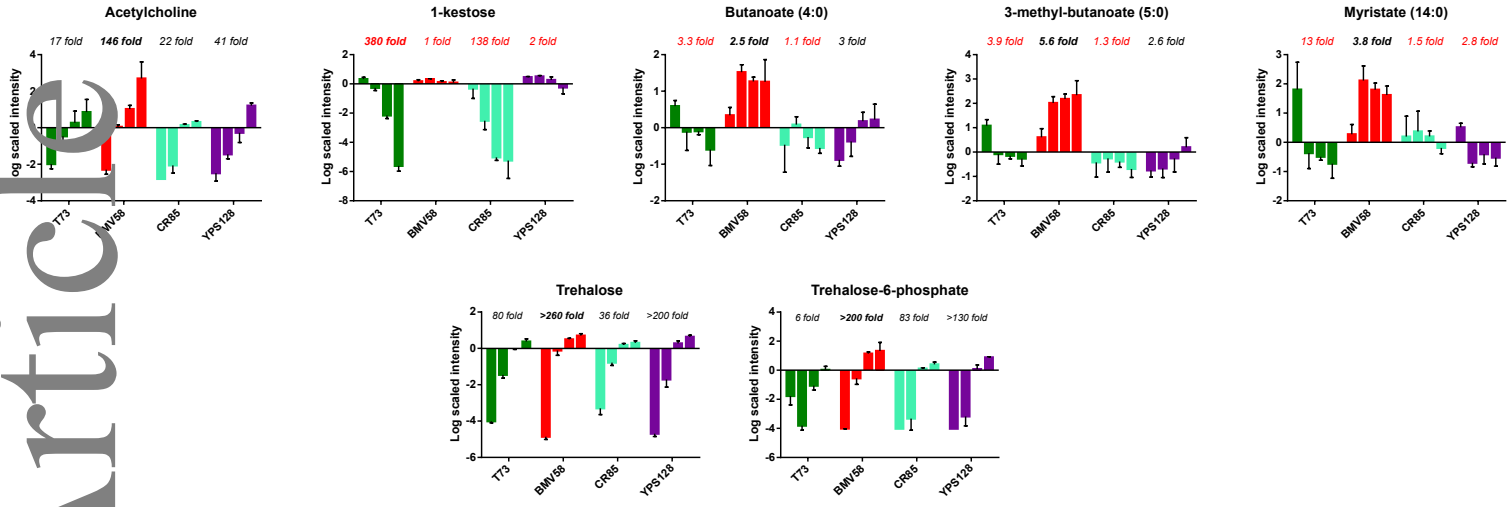

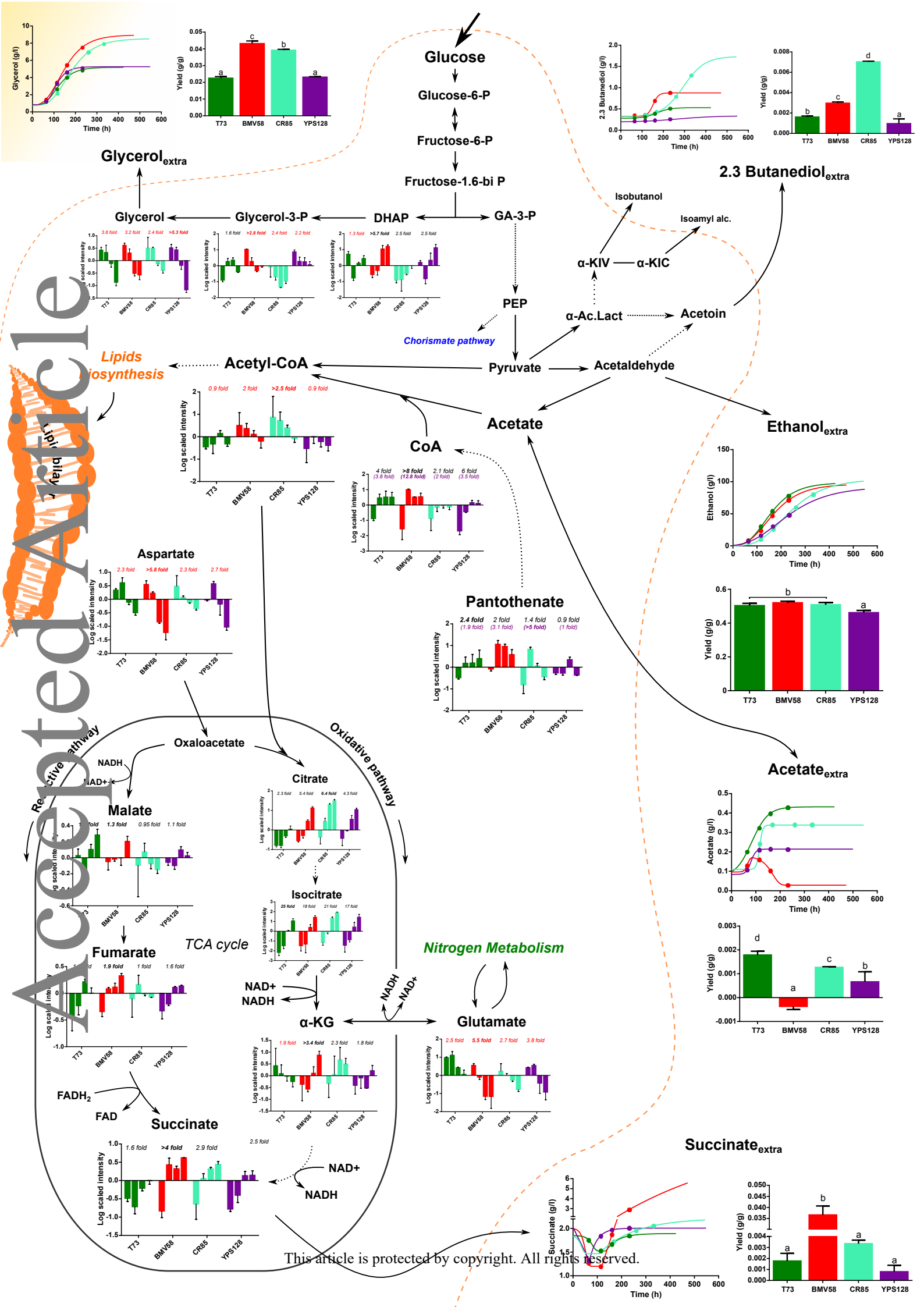

P.P pathway

6P-Glu-δ-lac

Xyl-5-P / Rib-5-P

Ery-4-P

Ribulose/Xylulose

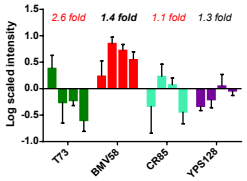

Glu-6-P

Glucose

Glycolysis

PEP

Pyruvate

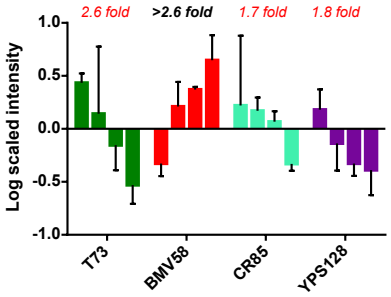

DAH-7-P

Erythritol$_{intra}$

Erythrose

Erythritol$_{extra}$

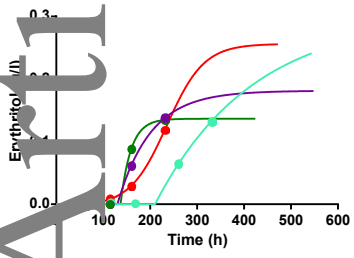

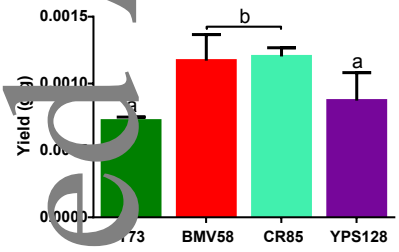

3-dehydroquinate

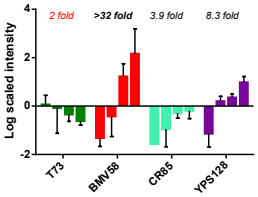

Quinate

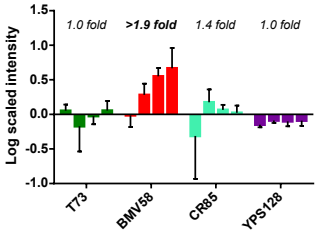

Chorismate pathway

3-dehydro-shikimate

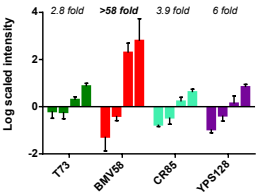

Shikimate

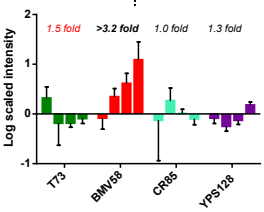

Tyrosine

Chorismate

Phenylalanine

Anthranilate

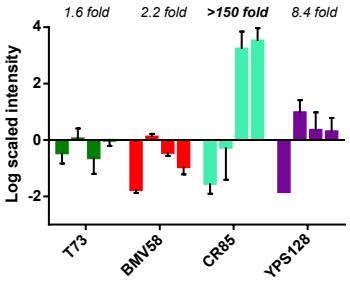

NAD de Novo synthesis

Tryptophan

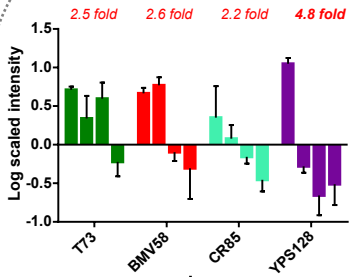

O_2

Kynurenine

O_2

Kynurenate

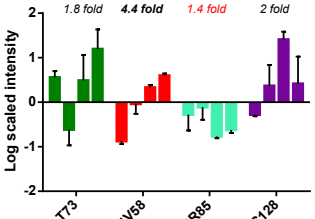

NAD+

Phenylpropanoids

Phenylacetate

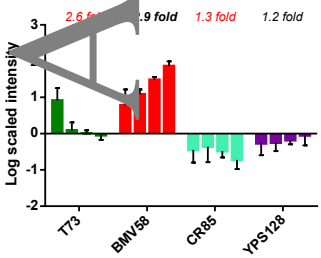

Phenyl lactate

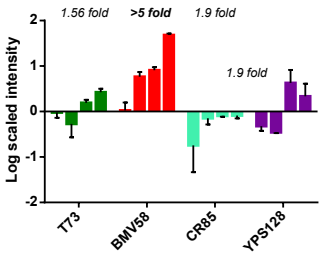

2-phenylethanol$_{extra}$

2-phenylethyl acetate$_{extra}$

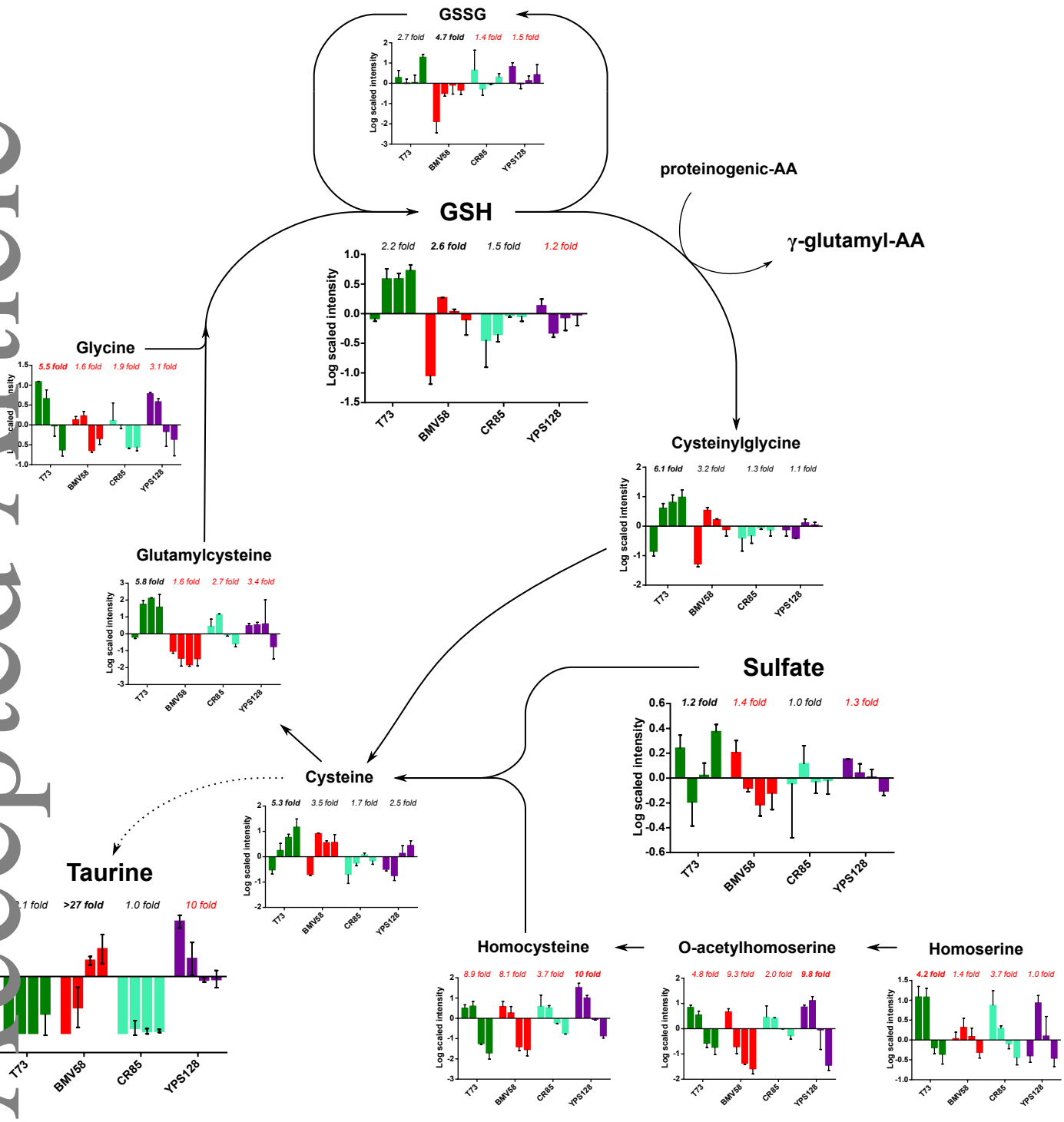

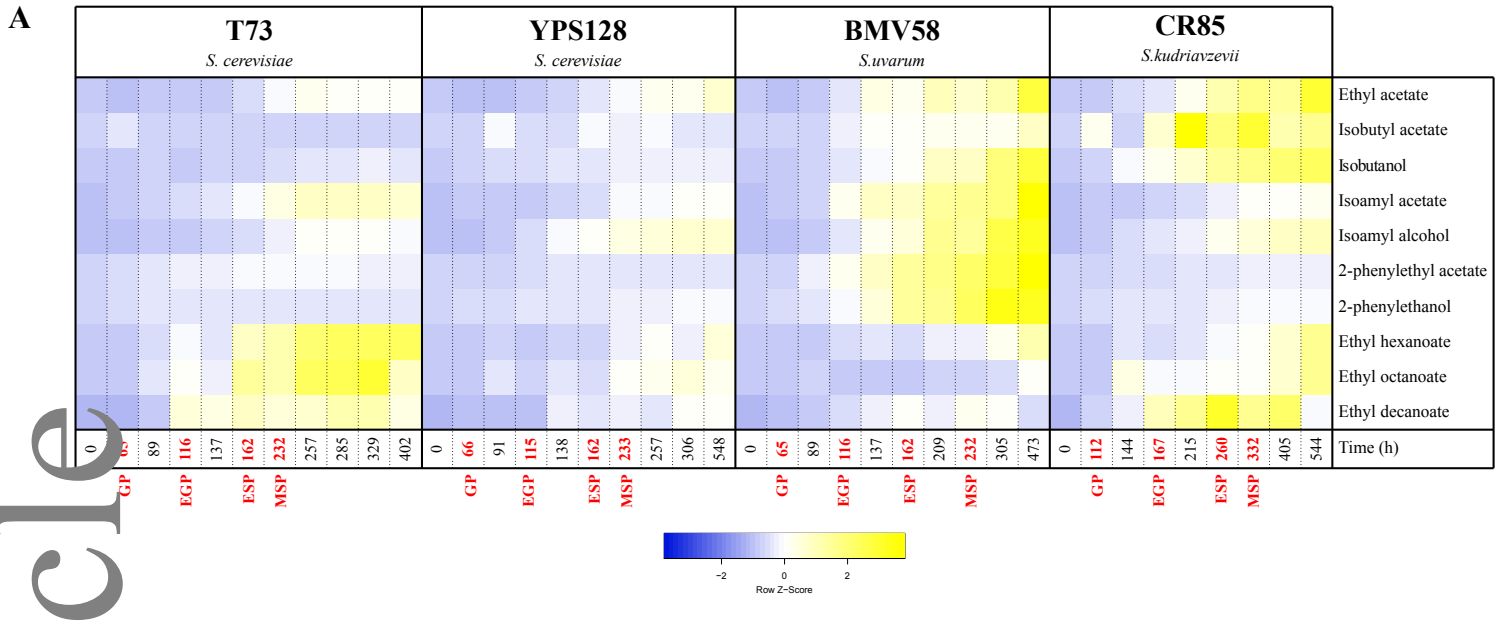

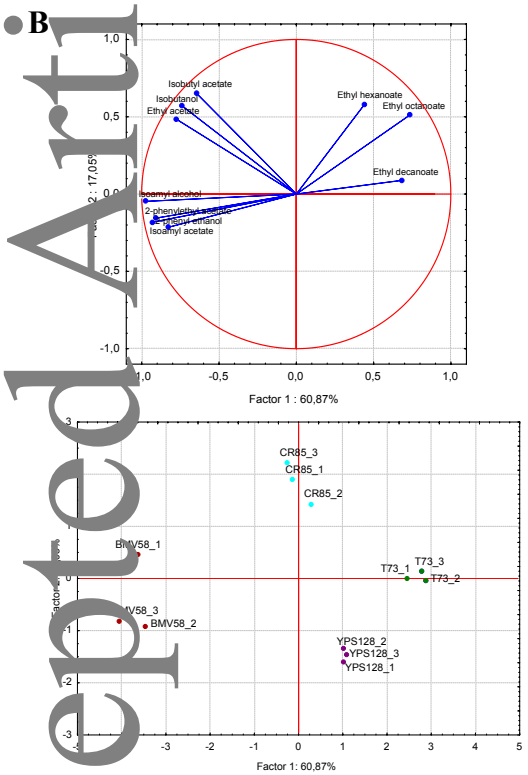

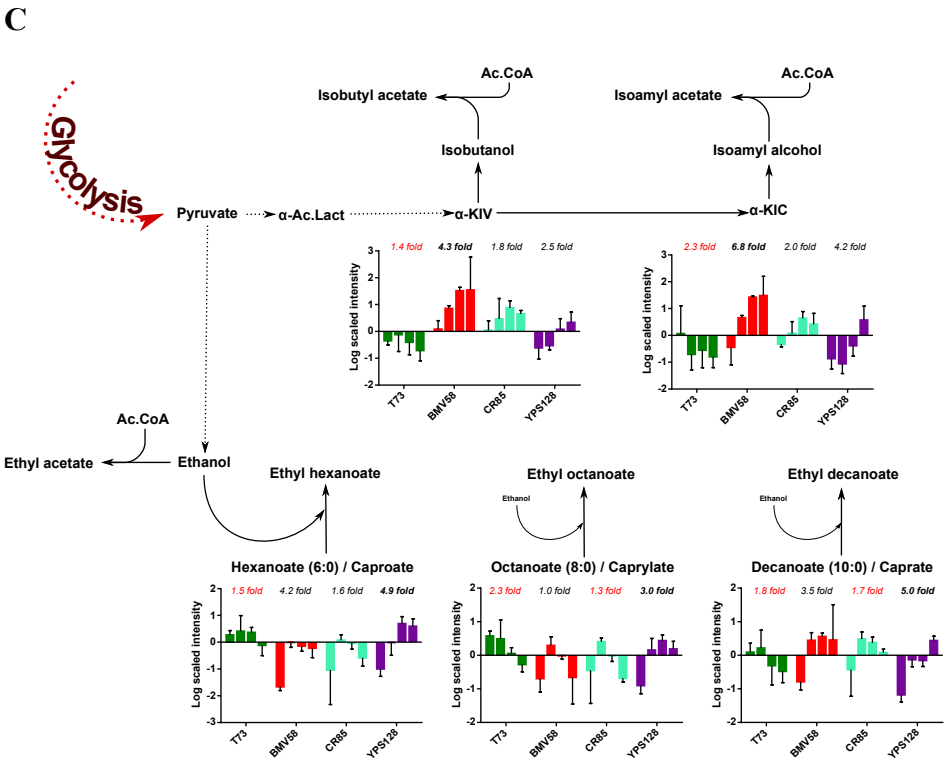

Table 1: Growth and fermentative parameters of the four strains at 12ºC

	T73 *S. cerevisiae*		**BMV58** *S. uvarum*		**CR85** *S. kudriavzevii*		**YPS128** *S. cerevisiae*	
	mean ± SE	**95% CI**	**mean ± SE**	**95% CI**	**mean ± SE**	**95% CI**	**mean ± SE**	**95% CI**
DW_{max} ($g.l^{-1}$)	3.9 ± 0.10	3.7 to 4.1 ^{b}	6.0 ± 0.2	5.6 to 6.4 ^{d}	2.9 ± 0.1	2.7 to 3.0 ^{a}	5.1 ± 0.2	4.7 to 5.5 ^{c}
μ_{max} (h^{-1})	0.082 ± 0.001	0.078 to 0.085 ^{c}	0.098 ± 0.002	0.092 to 0.10 ^{d}	0.053± 0.002	0.048 to 0.57 ^{a}	0.071 ± 0.002	0.067 to 0.074 ^{b}
λ (h)	12.6 ± 0.8	11 to 14 ^{a}	23.3 ± 0.8	22 to 26 ^{b}	24.3 ± 2.3	20 to 29 ^{b}	10.8 ± 1.2	8.5 to 13 ^{a}
r_{YAN} (h^{-1})	0.029 ± 0.006	0.015 to 0.043 ^{b}	0.034 ± 0.006	0.022 to 0.046 ^{b}	0.011± 0.002	0.0048 to 0.013 ^{a}	0.028 ± 0.005	0.020 to 0.042 ^{b}
T_{50} YAN (h)	62 ± 5.4	51 to 73 ^{a}	68.5 ± 3.0	62 to 75 ^{a}	121.4 ± 15	119 to 150 ^{c}	87.6 ± 3.7	82 to 95 ^{b}
g_{DW}/g_{YAN}	13.7 ± 0.4	12.9 to 14.4 ^{b}	18.8 ± 0.8	17.2 to 20.4 ^{c}	12.3 ± 0.2	11.9 to 12.8 ^{a}	19.3 ± 1.4	16.3 to 22.3 ^{c}
r_{Eth} (h^{-1})	0.52 ± 0.016	0.48 to 0.55 ^{d}	0.45 ± 0.012	0.43 to 0.47 ^{c}	0.39 ± 0.008	0.37 to 0.40 ^{b}	0.29 ± 0.017	0.25 to 0.32 ^{a}
Eth_{max} ($g.l^{-1}$)	97.9 ± 1.6	94 to 101 ^{a}	96.2 ± 0.98	94 to 98 ^{a}	103.9 ± 0.95	95 to 105 ^{a}	92.2 ± 3.4	85 to 99 ^{a}
r_{Gly} (h^{-1})	0.034 ± 0.0014	0.032 to 0.037 ^{a}	0.045 ± 0.0025	0.040 to 0.051 ^{b}	0.040 ± 0.0015	0.036 to 0.043 ^{a,b}	0.049 ± 0.003	0.042 to 0.055 ^{b}
Gly_{max} ($g.l^{-1}$)	4.38 ± 0.06	4.26 to 4.51 ^{a}	8.22 ± 0.24	7.73 to 8.71 ^{b}	7.79 ± 0.13	7.53 to 8.05 ^{b}	4.42 ± 0.10	4.21 to 4.63 ^{a}
r_{But} (h^{-1})	0.032 ± 0.006	0.020 to 0.044 ^{b}	0.078 ± 0.015	0.05 to 0.11 ^{c}	0.020 ± 0.001	0.018 to 0.022 ^{b}	0.011 ± 0.003	0.005 to 0.017 ^{a}
But_{max} ($g.l^{-1}$)	0.53 ± 0.01	0.51 to 0.54 ^{b}	0.88 ± 0.01	0.85 to 0.90 ^{c}	1.74 ± 0.02	1.7 to 1.8 ^{d}	0.34 ± 0.01	0.31 to 0.36 ^{a}
r_{A} (h^{-1})	0.030 ± 0.005	0.02 to 0.04 ^{a}	0.156 ± 0.163	0 to 0.53 ^{a}	0.158 ± 0.131	0 to 0.42 ^{a}	0.10 ± 0.02	0.06 to 0.13 ^{a}
Ac_{max} ($g.l^{-1}$)	0.43 ± 0.01	0.42 to 0.44 ^{d}	0.03 ± 0.004	0.02 to 0.03 ^{a}	0.34 ± 0.004	0.33 to 0.35 ^{c}	0.214 ± 0.004	0.20 to 0.22 ^{b}
r_{Succ} (h^{-1})	0.021 ± 0.006	0.009 to 0.033 ^{b,c}	0.0018 ± 0.0006	0.0005 to 0.003 ^{a}	0.0069 ± 0.0012	0.004 to 0.009 ^{b}	0.031 ± 0.007	0.016 to 0.046 ^{c}
$Succ_{max}$($g.l^{-1}$)	1.90 ± 0.02	1.85 to 1.93 ^{a}	5.63 ± 0.41	5.5 to 5.9 ^{c}	2.22 ± 0.04	2.1 to 2.3 ^{b}	2.00 ± 0.03	1.9 to 2.1 ^{a,b}
r_{Ery} (h^{-1})	0.045 ± 0.008	0.028 to 0.062 ^{b}	0.025 ± 0.004	0.016 to 0.034 ^{b}	0.0048 ± 0.001	0.0028 to 0.0068 ^{b}	0.014 ± 0.003	0.0076 to 0.021 ^{a}
Ery_{max} ($g.l^{-1}$)	0.14 ± 0.003	0.13 to 0.15 ^{a}	0.26 ± 0.01	0.23 to 0.29 ^{c}	0.24 ± 0.01	0.24 to 0.36 ^{c}	0.18 ± 0.01	0.16 to 0.20 ^{b}

Growth and fermentative parameters obtained by fitting models to biological data using non-linear regression. Best-fit parameters were determined minimizing the sum of squares of the difference between experimental data and the mathematical model using GraphPad Prism 6.0 Software. Parameters are presented as mean ± standard error (SE). For each parameter, a 95% confidence interval was approximated by using the estimated predictions and standard error. Parameters for which the confidence intervals do not intersect can be considered significantly different. Shared superscript letters (a, b, c) in the same row indicate no significant difference.

Abbreviations: DW_{max} (maximum dry weight biomass), μ_{max} (maximum growth rate), λ (lag phase), r_{YAN} (maximum consumption rate of YAN), T_{50} YAN (estimated time at which 50% of the total YAN content was consumed), g_{DW}/g_{YAN} (maximum biomass yield expressed as g of dry weight biomass produced/g of YAN consummed), r_{Eth} (maximum production rate of ethanol), Eth_{max} (maximum ethanol concentration at the end of fermentation), r_{Gly} (maximum production rate of glycerol), Gly_{max} (maximum glycerol concentration at the end of fermentation), r_{But} (maximum production rate of 2,3 butanediol), But_{max} (maximum 2,3 butanediol concentration at the end of fermentation), r_{Ac} (maximum production rate of acetate), Ac_{max} (maximum acetate concentration at the end of fermentation), r_{Succ} (maximum production rate of succinate), $Succ_{max}$ (maximum succinate concentration at the end of fermentation), r_{Ery} (maximum production rate of erythritol), Ery_{max} (maximum erythritol concentration at the end of fermentation).